

Dear Editor,

We have the pleasure to submit the revised version of the manuscript. We have implemented all the changes proposed in the response to the reviewers. The major changes concern a complete revision of the outline of the manuscript, while keeping its initial objectives. We also revisited the organization of the figures accordingly. We added figure 7 to enlarge the discussion on the linkages between the long term climate changes and the seasonal insolation forcing, figure 8 to show the changes in sea-ice and snow cover in the northern hemisphere, and figure 12 to quantify the southward shift of the African rainbelt and long term decrease in precipitation. We reduced the number of vegetation maps and keep those now in figure 10 to show the MH, PI and historical vegetation in the transient experiment, and in figure 16 to discuss the different vegetation states between our Vnone and Vmap simulations. A panel has been added in figure 5 to show the changes in insolation seasonality in the northern and the southern hemispheres. Figure 14 on the mega biome comparison now also include a comparison of the MH minus PI biomes.

We would like also to thank you for your comments. We provided a response to them below. We also include at the end of it the responses to the reviewers that are similar to the one we posted previously on the CP server.

We hope that you'll find the revision in agreement with the responses and in good shape for publication in climate of the past.

With our best regards

Pascale Braconnot, on behalf of the co-authors.

### **Response to the editor comments.**

There are only a few items that I would like to add.

*One of your topics addresses multiple vegetation states. This is, indeed, a fascinating subject. You mentioned papers by Victor Brovkin and me. Hence it would be interesting to see whether you also find the differences in tropical large-scale circulation (e.g., a shift in the velocity potential) between the different states.*

We do not find big climate differences in climate. A robust feature is the small interhemispheric different in temperature and thus on cross equatorial heat transport. But it is tiny and not significant. The metrics also tell that it is not possible to statistically distinguish the two simulations, even when considering 2 regions and different seasons. Because of this we didn't add much on the analysis of the climate part. Future work would require running an ensemble to fully test this vegetation instability.

*In your reply to reviewer 1 you mentioned that you would use the biomisation method to evaluate the different vegetation states. Perhaps I just mis-understood this point. It would be more appropriate to compare simulated vegetation patterns directly instead of diagnosing these patterns by using the indirect biomisation.*

The biomisation method is only used to compare with BIOME6000 reconstruction. All maps showing baresoil, grass and tree are from the original ORCHIDEE PFTs. We also added a table in the appendix to address reviewer 1 comment, that we could have compared the simulated PI PFTs with those of the 1860 map we use when vegetation is prescribed considering grid points without land use. We also included a similar comparison for the grid points with land use, to show the differences in MH vegetation with the dynamical vegetation compared to the 1860 map. We also insist on the fact that the differences include both model biases and MH climate-vegetation feedback.

*Reviewer 2 questions the use of constant aerosol forcing. The effect of changes in Holocene aerosol concentration is a topical question. (You mentioned the papers by Francesco Pausat, for example.) It seems that it is not at all clear what effect a change in mineral dust during the Holocene has had on Holocene climate and climate variability. The effect of mineral dust on precipitation, for example, strongly depends on the chosen values of optical properties of the aerosols.*

The aerosols forcing we use is what is usually done in past climate simulations. There is nothing particular, except that we have to explain our choice to only consider dusts and sea-salt. We added a sentence to fully justify our choice by the fact that the effect we introduce by doing this on the mean climate is larger than the effect we expect from the change in MH dust. We agree that the question of MH dust is a complex topic. We mention several papers that consider dusts just to tell this is an open question. Pausat et al s study should be considered as an extreme oversimplified test case. It is interesting, but cannot be considered as realistic, but we made no particular comment in the text, because we are not looking at dust in details

*Reviewer 2 also mentions the calendar problem. Looking at the recent paper by Bartlein and Shafer (see GMD Discuss.), the effect can be pretty large, if monthly means are concerned. Averaging over 4 months should have a smaller effect. Perhaps you can cite your 1997 paper with Sylvie Jousaume?*

Thank you for this remark. Yes we added the reference to Jousaume and Braconnot 1997, and we hope it is clear that we only look at effects that would emerge whatever the calendar we use for this period.

*Line 35 of your manuscript: the term 'intertropical convergence zone' might be misleading, if you want to refer to the tropical rainbelt – see Sharon Nicholson's critique which appeared in BAMS, Feb. 2018, pp. 337.*

Normally now rain belt is used when referring to precipitation over land.

*Lines 69 ff: model biases: You are right that an atmosphere-ocean GCM is a different model than an atmosphere-ocean-vegetation model. Looking at the Holocene West African monsoon, I would argue that the biases of an atmosphere-ocean GCM are larger than that of an atmosphere-ocean-vegetation model. The former generally produces too small monsoon rain than the later. But can you really compare the biases of different model types?*

A difficult question. We are not able and do not do it. We only show how big they are using the metrics. This is an important point for model-data comparison, knowing that adding degrees of freedom in general degrade the simulated climatology, but not necessarily the mechanisms of

climate change. The last sentence of the text is on the need to develop methodologies to evaluate processes rather than climatological variables.

*Line 78: A word on why you start at 6ka would be sensible. It is the old problem: the Holocene climate around 6ka reveals pretty strong changes.*

We didn't comment much on this in the text, because we start from the well-established PMIP simulations. At least the ocean component is closer to present day conditions, so that we do not have to care too much of the ocean initial state, and 1000 year Mid-Holocene simulations were long enough to initialize the whole system. We have this question somehow for any period outside the modern range.

## Response to Reviewer 1 comments

Reviewer 1 provided several important comments on the structure and the objectives of the manuscript. The major recommendation is

*"I recommend to restructure the manuscript. The time-slice experiments must be embedded more strongly in the results of the transient simulation and a clear link must be established between the simulations. To reduce the number of experiments and figures, the simulations dealing with finding an appropriate initial state or discussing the differences to the PMIP3-CMIP5 model could be shifted to the Appendix. These are technically interesting but seem not to follow any scientific question. The result section of the transient simulations should be extended and more specified. In addition, research questions and aims of the study should be worked out to give the results a clear framework."*

We agree while reading these remarks that the original outline of the manuscript doesn't put enough emphasis on the transient simulation and that it would be better to construct the outline of the paper so as to better echo the title. It is important for us to keep the discussion of the different sensitivity tests. This knowledge is needed to properly analyze the results of the transient simulation and to know what we can or cannot expect from it. We will add a few results on the transient simulations. But we'll keep most of the content as it is. To better emphasize the results of the transient simulations we propose to restructure the manuscript as follow:

1. Introduction
2. Model and experiments
3. Simulated climate and vegetation throughout the mid to late Holocene
4. Multiple vegetation states and uncertainties
5. Conclusion

Compared to the original outline:

1. Introduction
2. Model, mid Holocene and preindustrial experiments
3. Mid-Holocene simulations with interactive vegetation

4. Simulated climate and vegetation throughout the mid to late Holocene
5. Conclusion

The new structure is a response to the reviewer comment to provide a clear framework for the results. The new section 2 will start from the experimental design of the transient experiment; so as to explain that the mid-Holocene is the reference period and only a subset of simulations were run for the pre-industrial period. The discussion of the sensitivity tests will be slightly refocused and redistributed in the different subsections. The discussion on the MH initial vegetation state will be included, but not the discussion on the multi vegetation states for the PI vegetation. The current section 3 on mid-Holocene simulations will thus be redistributed between section 1, and section 4 where a specific focus will be put on the multiple vegetation states for PI and the evaluation of the simulated vegetation for MH and PI using the biomisation method. This is a way to discuss what we call limits in the title. In the new section 3 on the transient simulation we'll slightly enlarge the analysis of the response to the insolation forcing and add a discussion on the climate variables at the regional scales.

The different figures will be reorganized so as to reflect the new outline. It sounds difficult to reduce the number, but we'll find a way to have fewer maps with vegetation changes. It requires some work, but it should be easily done, thanks to the way we organized the model outputs needed to prepare this manuscript.

We also would like to thank reviewer 1 for the list of minor comments that are useful to improve the manuscript.

All the editing comments have been taken into account and already added in the text before any change is made. We provide below some responses for the other comments

*L130: what do you mean with 'transient late Holocene simulation'*

The last 6000 years (I.E from -6000 BP to 0k = 1950 for insolation). This will be stated more clearly in the text

*L243: Please explain the metrics in more detail (e.g. in the Appendix) because the metric package may be unknown to the readers*

A paragraph will be added in the appendix to better explain what is computed

*L314: The heading of chapter 3 is: 'mid-Holocene simulations' so why is there a section dealing with pre-industrial climate?*

We hope it will be less misleading in the new outline. The point is to know how good is the model quite early in the text. In the new version we decided to evaluate the "climate" in section 2 and have the discussion on "vegetation" in section 4. This should better insist on the fact that we have active dynamical vegetation in this simulation and that considering climate or vegetation evaluation can lead to different conclusions on the realism of the simulation depending on the way the evaluation is done.

*L319-320: I do not understand what is meant by 'vegetation biases' in this context. When vegetation is interactive, the calculated vegetation distribution can be biased, but how does this bias impact the representation of the simulated vegetation? Please clarify.*

We only have in mind the biases coming from climate-vegetation feedbacks that amplify the known bias of the model when dynamical vegetation is switched off. We are not in a position where we can tell how the bias in the vegetation model affects the full coupled system.

*L337: What do you mean by this? that the differences in PI simulations are of similar magnitude as the differences between PI and MH ?*

Since the vegetation maps are similar in Vmap and Vnone for MH, the difference in PI vegetation between Pi-Vmap and PI-Vnone explains the difference in MH-PI vegetation calculated using the Vmap simulation or the Vnone simulation. We'll revisit the way we discuss it.

*L383: ' : : follow the long term insolation changes in each hemisphere: : ' What about SH Winter? Please be more precise.*

We'll add a discussion on this point, but focusing on the seasonal cycle and the seasonality of the insolation forcing. For the northern regions and the southern hemisphere, part of the answer is in the ocean heat storage and the other part is in the sea-ice and snow cover.

*L409: It seems as if the tree fraction follows the summer insolation change. Please specify and explain. What about the annual mean changes in temperature, precipitation and insolation?*

We will add a short discussion on temperature and precipitation, but for the 3 regions we consider later in the text, considering, min, max and annual mean monthly temperatures and precipitations as well as sea-ice and snow cover for the region north of 60°N and Eurasia.

*L456: What do you mean by 'rapid changes' and if these 'deserve attention' why don't you investigate them in this study?*

We should have included these remarks in the conclusion. It is out of the scope of this paper. So we'll refocus the text.

*L476-477: Is there a possibility to figure out the reasons for having different PI climate-vegetation changes?*

We provide all what we know and the possible caveat in the manuscript. Going further requires a new study and certainly another 1 to 2 years to do it properly with ensemble sensitivity tests. We already checked all what we could check in the last 2 years about it. This is also why it is important for us to show it and discuss it in the manuscript. It can be "by chance" or linked to amplification of small differences in the initial state under modern conditions.

*-L581: Isn't it originally the method of Prentice et al. 2011? What is different to the method of Zhu et al. 2018?*

Yes, the algorithm follows Prentice et al. (2011), with thresholds prescribed as in Zhu et al. (2018). We also tested the different threshold values reported in Figure A2.

We will revise this sentence as: “To convert the modelled PFTs by ORCHIDEE into mega BIOMES, we use the algorithm proposed by Prentice et al. (2011). Figure A2a shows the different threshold values tested in this algorithm, with the black numbers corresponding to the default values used to produce Figure 7 in the main text.”

*-L590: It is not obvious why the GDD limit of 500\_C is being tested, are these values realistic? I guess ORCHIDEE also uses a GDD limit of > 350\_C for the existence of boreal trees vs. tundra (GDD<350\_C). A biomisation using a GDD limit of 500\_C thus may not represent the vegetation simulated by the model, because it suggest tundra in regions that are suited for forests.*

The threshold of 500 °C days is tested because it was used in Joos et al. (2004) to convert LPJ-simulated PFT fractions into biome types. ORCHIDEE intrinsically does not use a simple GDD limit to constrain the existence of boreal tree PFTs. GDD thresholds are only used in the phenology module to determine the onset time of leaves, while their values are PFT-specific and are also modulated by the dormancy period, which varies for the same PFT located in different grid cells (see more details in Krinner et al., 2005). By influencing leaf onset, GDD values impact photosynthesis and growth of the PFT, and then indirectly affect establish/mortality rates and finally abundance of this PFT in ORCHIDEE. The biomisation algorithm is just a post-processing of the fractional PFT outputs of ORCHIDEE, with some broad-scale empirical thresholds. Therefore, we do not think testing a value of 500 °C days here would be “incompatible” to ORCHIDEE-simulated vegetation.

*-L598-599: Should we now reconsider the choice of bioclimatic limits in the DGVMs?  
- What about data availability?*

As mentioned above, GDD is not a direct bioclimatic limit inside ORCHIDEE. Furthermore, although changing the GDD limit to 500 °C days improves the metric for tundra in Figure A2b, we should keep in mind that (1) any bias in simulated temperature will also affect the biomisation result and thus the “correctness” compared with the pollen data; and (2) the expansion of tundra over woodland in the case of “GDD=500” compared to “Default” might actually degrade the biome distribution, which cannot be reflected in the “correctness” metric because of limited pollen data in middle Siberia (this is why we mentioned data availability).

*-Fig.4: Why are MH\_Vnone and MH\_Vmap so different?*

We are not sure we fully understand the question. These simulations start with very different initial state for the land surface model. So it reflects different adjustment time, and the curve show they converge to the same solution. So we would rather say that they are very similar and not different.

*Fig.7: It should be explained, why there is Savanna in the northern latitudes. In my print, the pink and orange color is not really distinguishable. Please state, why there is no grassland in North Africa in your simulation*

As shown in Figure A2a, “savanna and dry woodland” is defined if the foliage projective cover (a combination of simulated fractional coverage and leaf area index) is high but average tree height is not enough. Since tree height is mainly determined by woody biomass in ORCHIDEE, we speculate that a potential underestimation of tree biomass in the model might lead to the replacement of boreal forests with woodlands in the high latitudes. This could be because of bias in climate and/or

bias in ORCHIDEE in terms of photosynthesis or carbon allocation scheme. We will add these discussions in the corresponding text.

For North Africa, the model simulates desert instead of grasslands. This is mainly because of amplification by the climate-vegetation feedback of the underestimated precipitation in this region.

We will change the colors to make them more distinguishable in the revised manuscript.

*-Fig.9: Maybe this figure could be moved to the Appendix*

We will keep this figure in the text and add to it a panel with the seasonal change in incoming solar radiation at TOA in both hemispheres. Showing the forcing we use in the simulation over the 6000 years is important for the discussion. We'll also better emphasize in the text the result of the last period.

*-Fig.10: When looking into palaeo-seasons, one always faces the problem of different calendars. The months NDJF or JJA differ in length between mid-Holocene and PI. It should at least be mentioned in the text and in the caption, that this 'problem' exists and is not considered, neither by the model nor in the analysis. But this problem may change the trends discussed here!*

In practice the effect of calendar over the mid Holocene is small. Jousaume and Braconnot 1997 show it is 5 days at most for the difference in the date of the Autumnal equinox when March 21 is prescribed as the reference date for the vernal equinox in all simulations. We are averaging on long time and show the long term trends, discussing only the significant results. The larger analysis biases resulting from the calendar are found in autumn. We do not discuss this particular season. Our conclusions, given what we are doing here will not be altered by the calendar effect. But we recognize that we need to keep this in mind. For other periods, when eccentricity is larger, this would not be the case.

*-Fig.11: it is 'Northern Hemisphere'. It would also be interesting, how the simulated tree cover and bare-soil fractions at the end of the simulation compare to modern estimates on (natural) tree cover. How large is the underestimation of forest in the high northern latitudes by the model?*

We agree it would be interesting, but we are also concerned that because we do not have land use in the simulations. Land use has an impact at regional scale. However we also know, and this is shown in the MH biome comparisons, that the differences between the simulated vegetation and the real world are larger than differences that would come from land use. Since we decided now to add a biome comparison for PI using pollen data for 0k, we'll consider this remark in the revision. We'll also reinforce the discussion and questions about the evaluation of the vegetation we simulate out of such transient simulation.

*Fig.12: What causes the strong peak around 4.8ka ?*

This event comes from internal noise and/or compound variability events, superimposed on the long term trend induced by the insolation forcing. There is no obvious cause. We checked that it doesn't come from an artificial computing failure when running the simulation.

## Response to Reviewer 2 comments

Review 2 has very strong comments on the content and the organization of our manuscript.

*"I recommend modifying the structure and results to better reflect the target audience. You can leave the model development and testing sections, but you need to provide additional context and analyses."*

« General Comments:

*The results and analyses left me unsatisfied, especially given the amount of time spent on model testing. Many findings are dismissed as beyond the scope of this paper or for future work. However, without in-depth exploration of at least some of the interesting results of the simulations, the paper feels more like a data description, which is fine, but not especially appropriate for Climate of the Past. I recommend expanding the transient simulation results and analysis, since it is the novel part of this study. There are several topics that could be explored further, such as the importance of dynamic vegetation in the transient climate response (needed for the title), the mechanisms driving multiple equilibria, and comparison with proxy reconstructions. The authors might also want to consider how do these results compare with other transient model simulation?"*

Some of these comments are consistent with those of reviewer 1. We realize that the structure we adopted for this manuscript deserved us. We already provided quite a lot of in depth analyses even though we agree that the section on the transient simulation as it is appears a little bit descriptive. We propose to add a few things on the transient simulation to better discuss the response to the insolation forcing and the linkage between climate and vegetation at the regional scale. But we will keep our initial focus and use the different tests we did to highlight the context in which the simulation can be considered, in particular for future model-data comparisons. This implies that we better highlight the limits we discussed. They come from the possibility of multi-states for vegetation, model biases and caveats for model evaluation on the pre-industrial or the historical period. We thus propose to reorganize the manuscript so as to have the discussion of these points in the last section. This will allow us to better connect the different pieces and provide a more focused manuscript.

To better emphasize the results of the transient simulations we propose to restructure the manuscript as follows:

6. Introduction
7. Model and experiments
8. Simulated climate and vegetation throughout the mid to late Holocene
9. Multiple vegetation states and uncertainties
10. Conclusion

Compared to the original outline:

6. Introduction
7. Model, mid Holocene and preindustrial experiments
8. Mid-Holocene simulations with interactive vegetation
9. Simulated climate and vegetation throughout the mid to late Holocene
10. Conclusion



As stated above, the new structure is a response to the reviewer request to revisit the structure of the manuscript. The new section 2 will start for the experimental design of the transient experiment; so as to explain that the mid-Holocene is the reference period and that only a subset of simulations was run for the pre-industrial period. The discussion of the sensitivity test will be slightly refocused and redistributed in the different subsections. The construction of the MH initial state for vegetation will also be included, but not the discussion on the possibility for multi vegetation states for PI. The current section 3 on mid-Holocene simulations will thus be redistributed between section 1, and section 4 where a specific focus will be put on the multiple vegetation states for PI and the evaluation of the simulated vegetation for MH and PI using the biomisation method. We'll also emphasize what we call limits in the title. In the new section 3 on the transient simulation we'll slightly enlarge the analysis of the response to the insolation forcing and add a discussion on the climate variables over the three regions.

The different figures will be reorganized so as to reflect the new outline. It sounds difficult to reduce their number, but we'll find a way to have fewer maps with vegetation changes.

Responses to the other comments. The comments dealing with text editing will be considered if still relevant in the revised version of the manuscript. We answer only to questions or to comments considering the content.

*Line 123: Can sea level actually change in the model?*

The ocean model has a free surface. The average sea level evolves with the global surface water budget (evaporation – precipitation – river runoff – water flux from ice sheet). However, the numeric is not designed for sea level large sea level change. It's better to keep it small with regards to the depth of the first level (10 m). The water conservation in the coupled model is thus critical for sea-level stability and to make sure that the sea-level change in a transient experiment is indeed the result of climate changes and not of model spurious drift.

*Line 143: I do not think that this is very good justification for not thoroughly testing modifications against preindustrial climate.*

We do not fully understand this comment. We provide comparison for PI for a subset of simulations. The argument on computing time is only the truth and we had to adjust our strategy to the computing allocation we had. We didn't had enough computing time to run both 1000 years long simulation on MH and PI for all the tests. We started the model developments on PI and then move on MH for the final tests that are presented here that all requested long simulations.

*Lines 152-153: Given the importance of the aerosol responses, why do you prescribe aerosols here? Are dust and sea-salt prescribed to PI? How might this impact climate? I do not find “: :we also plan to run simulations with fully interactive dust and sea-salt” good justification.*

Here also we do not fully understand this comment. We wrote: because we are developing the interactive version with aerosols that can be run on 6000 year long time periods. What we didn't write is that is also requires developing the full coupling with the interactive vegetation for the dust sources, and that we are here at the first step with dynamical vegetation. It is ongoing work. That would require another 1 to 2 years. Aerosols are set to their pre-industrial values, and they are fully interactive with the radiative code in the atmosphere.

*Line 163: Some of these modifications do not feel robust (e.g. the soil evaporation factor). They are, we only show robust results here.*

*Lines 175-176: What is the TOA energy imbalance for these runs? This could be important since different simulations are run for different amounts of time. 0.4 Wm<sup>-2</sup> is far from zero: : :*

The imbalance is negligible  $\sim 0$  (with interannual variability around it). Of course, during the adjustment phase, it is equivalent to what is shown at the surface. Part of the small offset at the surface results from small errors when estimating the heat budget from the monthly model outputs. It is not possible from the limited output we kept for the long simulations to properly reallocate the right latent heat values when we are dealing with evaporation or sublimation on surfaces with evolving sea ice or snow. This is done properly during the model run. It is thus mostly a diagnosis error rather than a model imbalance. Note however that interannual variability is of the order of 0.2-0.4 W/m<sup>2</sup>.

*Line 181: Why does this modification impact the ocean response so dramatically? I thought the hydrologic modification should only impact the land surface. Am I missing something?*

Because we are in a coupled system and that energy is redistributed between land and ocean. Changes in evaporation over land affect moist static energy and its gradients.

*Line 310: how well does 50% compare with other models?*

We will conduct the same biomisation and evaluation against pollen data for PI outputs. This would provide a comparison of model performance in vegetation distribution under different climates. For other models, say PMIP3 outputs, it is difficult because the biomisation algorithm requires some variables (e.g. tree height) that are not usually uploaded in PMIP3. We will, however, add more discussions here about the model-data evaluation, referring to the recent work of Dallmeyer et al., (2018, CPD).

*Lines 325-326: "Since surface variables adjust rapidly, this is a way to compare the rapid adjustment to insolation 326 and the additional effect due to the dynamical vegetation (not discussed here)." Why say this then? It feels like an advertisement: : :*

We agree it is not needed.

*Line 380: Do you mean JJAS? How do you account for the calendar changes?*

We don't account for calendar change. See response to reviewer 1. The changes are limited, even though present over the last 6000 years. Here, we only discuss robust features that would emerge whatever the choice of calendar. We'll add a caution mark on the calendar in the revised version.

*Line 398: Interesting: : :Worth performing spectral analysis on the variability?*

Certainly, we agree, but later and not in this manuscript. It is a subject per se.

*Lines 418-419: Why would this lead to an underestimate?*

Even though the carbon cycle is interactive in the land surface and in the ocean, the fact that the carbon concentration is imposed in the atmosphere in the model prevents carbon feedback between the different reservoirs. Model forced in emission rather than concentrations have a larger range of response in their carbon cycle. This is why we think that in a simulation with where emissions interact with the atmospheric concentration could lead to different results. The wording here was misleading. Underestimated was there to mean not fully computed and that in a fully interactive model the results could be different. We'll revisit the sentence to better reflect what we want to say.

Summary  
27/02/2019 17:18:22

Differences exist between documents.

**New Document:**

[Braconnotetam\\_CP-2018-140\\_vrev](#)

47 pages (3.91 MB)

27/02/2019 17:17:31

Used to display results.

**Old Document:**

[cp-2018-140-supplement](#)

44 pages (3.97 MB)

27/02/2019 17:17:30

[Get started: first change is on page 1.](#)

No pages were deleted

## How to read this report

**Highlight** indicates a change.

**Deleted** indicates deleted content.

 indicates pages were changed.

 indicates pages were moved.

1

## 2 **Strength and limits of transient mid to late Holocene** 3 **simulations with dynamical vegetation**

4 Pascale Braconnot\*, Dan Zhu, Olivier Marti and Jérôme Servonnat

5 IPSL/Laboratoire des Sciences du Climat et de l'Environnement, unité mixte CEA-CNRS-UVSQ,  
6 Université Paris Saclay, Bât. 714, Orme de Merisiers, 91191 Gif-sur-Yvette Cedex.

7 *Correspondance to* : pascale.braconnot@lsce.ipsl.fr

8 **Abstract.** We present the first simulation of the last 6000 years with a version of the IPSL Earth System  
9 model that includes interactive dynamical vegetation and carbon cycle. It is discussed at the light of a set of mid  
10 Holocene and pre industrial simulations performed to set up the model version and to initialize the dynamical  
11 vegetation. These sensitivity experiments remind us that model quality or realism is not only a function of model  
12 parameterizations and tuning, but also of experimental set up. The transient simulations shows that the long term  
13 trends in temperature and precipitation have similar shape to the insolation forcing, except at the equator, in high  
14 latitudes and south of 40°S. In these regions cloud cover, sea-ice, snow, or ocean heat content feedbacks lead to  
15 smaller or opposite temperature responses. The long term trend in tree line in northern hemisphere is reproduced  
16 and starts earlier than the southward shift vegetation over the Sahel. Despite little change in forest cover over  
17 Eurasia, a long term change in forest composition is simulated, including large centennial variability. The rapid  
18 increase of atmospheric CO<sub>2</sub> in the last centuries of the simulation contributes to enhance tree growth and  
19 counteracts the long term trends induced by Holocene insolation in the northern hemisphere and amplify it in the  
20 southern hemisphere. We also highlight some limits in the evaluation of such a simulation resulting from model  
21 climate-vegetation biases, the difficulty to fully assess the result for pre-industrial or modern conditions that are  
22 affected by land-use, and the possibility for multi-vegetation state under modern conditions.

### 23 **1 Introduction**

24 Past environmental records such as lake levels or pollen records highlight substantial changes in the  
25 global vegetation cover during the Holocene (COHMAP-Members, 1988; Wanner et al., 2008). The early to  
26 mid-Holocene optimum period was characterized by a northward extension of boreal forest over north Eurasia  
27 and America which attests for increased temperature in mid to high latitudes (Prentice and Webb, 1998). A  
28 massive expansion of moisture and precipitation in Afro-Asian regions has been related to enhance boreal  
29 summer monsoon (Jolly et al., 1998; Lezine et al., 2011). These changes were triggered by latitudinal and  
30 seasonal changes in top of the atmosphere (TOA) incoming solar radiation caused by the long term variation in  
31 Earth's orbital parameters (Berger, 1978). During the course of the Holocene these features retreated towards  
32 their modern distribution (Wanner et al., 2008). While global data syntheses exist for the mid-Holocene (Bartlein  
33 et al., 2011; Harrison, 2017; Prentice et al., 2011), reconstructions focus in general on a location or a region  
34 when considering the whole Holocene. For example regional syntheses for long term paleo records over Europe  
35 reveal long term vegetation changes that can be attributed to changes in temperature or precipitation induced by  
36 insolation changes (Davis et al., 2003; Mauri et al., 2015). Similarly, over West Africa or Arabia, pollen data

37 suggests a southward retreat of the intertropical convergence zone (Lezine et al., 2017), and a reduction in North  
38 African monsoon intensity (Hély and Lézine, 2014). The pace of these changes varies from one region to the  
39 other (e.g. Fig. 6.9 in Jansen et al., 2007; Renssen et al., 2012) and has been punctuated by millennium scale  
40 variability or abrupt events (deMenocal et al., 2000), for which it is still unclear that they represent global or  
41 more regional events. How vegetation changes have been triggered by this long term climate change and what  
42 has been the vegetation feedback on climate is still a matter of debate.

43 Pioneer simulations with asynchronous climate-vegetation coupling suggested that vegetation had a  
44 strong role in amplifying the African monsoon (Braconnot et al., 1999; Claussen and Gayler, 1997; de Noblet-  
45 Ducoudre et al., 2000; Texier et al., 1997). When dynamical vegetation model were included in fully coupled  
46 ocean-atmosphere-sea-ice models, climate simulations suggested a lower magnitude of the vegetation feedback  
47 (Braconnot et al., 2007a; Braconnot et al., 2007b; Claussen, 2009). Individual model results indicates however  
48 that vegetation plays a role in triggering the African monsoon during mid-Holocene (Braconnot and Kageyama,  
49 2015), but also that soil moisture might play a larger role than anticipated (Levis et al., 2004). Reduced dust  
50 emission with increased vegetation and changed soil properties have been shown to amplify monsoon changes  
51 (Albani et al., 2015; Egerer et al., 2017; Pausata et al., 2016). In high latitude as well, the role of the vegetation  
52 feedback is not fully understood. Previous studies showed that the response of vegetation in spring combined to  
53 the response of the ocean in autumn were key factors to transform the seasonally varying insolation forcing into  
54 an annual mean warming (Wohlfahrt et al., 2004). The magnitude of this feedback has been questioned by Otto  
55 et al. (Otto et al., 2009), showing that vegetation was mainly responding to the ocean and sea-ice induced  
56 warming over land. The role and magnitude of the vegetation feedback were also questioned over Asia  
57 (Dallmeyer et al., 2010). The variety of response of dynamical vegetation models to external forcing is an issue  
58 in these discussions. However they all produce increased vegetation in Sahel when forced with mid-Holocene  
59 boundary conditions, which suggests that, despite large uncertainties, robust basic response can be inferred from  
60 current models (Hopcroft et al., 2017). Other studies have highlighted that there might exist several possible  
61 vegetation distribution at the regional scale for a given climate that can be related to instable vegetation states  
62 (e.g. Claussen, 2009). This is still part of the important questions to solve to fully explain the end of the African  
63 humid period around 4000-5000 years BP (Liu et al., 2007).

64 It is not clear yet that more comprehensive models and long Holocene simulations can help solve all the  
65 questions, given all the uncertainties described above. But they can help to solve the question of vegetation-  
66 climate state and of the linkages between insolation, trace gases, climate and vegetation changes at global and  
67 regional scales. For this, we investigate the last 6000 years long term trend and variability of vegetation  
68 characteristics as simulated by a version of the IPSL model with an interactive carbon cycle and dynamical  
69 vegetation. Off line simulations, using the original scheme for dynamical vegetation of ORCHIDEE, were  
70 already used to analyze Mid-Holocene and LGM vegetation (Kageyama et al., 2013b; Woillez et al., 2011). This  
71 has not yet been done in the fully coupled system for long transient simulations. Previous studies clearly  
72 highlight that small differences in the albedo or soil formulation can have large impact on the simulated results  
73 (Bonfils et al., 2001; Otto et al., 2011). Given all the interactions in a climate system, the climatology produced  
74 by a model version with interactive vegetation is by construction different from the one of the same model with  
75 prescribed vegetation. In particular model biases are in general larger (Braconnot and Kageyama, 2015;  
76 Braconnot et al., 2007b), so that the corresponding simulations need to be considered as resulting from different

77 models (Kageyama et al., 2018). The way the external forcing is applied to the model can also lead to  
78 climatology or vegetation differences between two simulations with the same model. It is thus important to know  
79 how the changes we made to the IPSL climate model to set up the version with dynamical vegetation affect the  
80 results and the realisms we can expect from the transient simulations. We thus investigate first how the major  
81 changes and tuning affect the mid-Holocene simulations and the performances of the model compared to  
82 simulations with the previous model version IPSLCM5A (Dufresne et al., 2013; Kageyama et al., 2013a).  
83 Several questions guide the analyses of the transient experiment. Is the long term response of climate and  
84 vegetation a direct response to the insolation forcing? How large is the impact of the trace gases? How different  
85 is the timing of the vegetation in different regions? Do we need to care about variability over such a long time  
86 period? We also need to put the responses to these questions in perspective with the level of realism we can  
87 expect from the simulated vegetation in such a simulation. It concerns the model biases, the compatibility  
88 between the climate and vegetation states produced by the transient simulation or obtained from snap shot  
89 experiments. Also different strategies can be used to initialize the vegetation dynamics and produce the mid-  
90 Holocene initial state for the transient simulation. We investigate if they have an impact on the simulated  
91 vegetation distribution.

92 The remainder of the manuscript is organized as follow. Section 2 describes the experimental set up, the  
93 characteristics of the land surface model as well as different model adjustments we made, and the initial state for  
94 the dynamical vegetation. Section 3 presents the transient simulation focusing on long term climate and  
95 vegetation trends at global and regional scales. Section 4 discusses the realism of the simulated vegetation and  
96 different sources of uncertainties that can affect it, before the conclusion presented in section 5.

## 97 **2 Model and the suite of experiments**

### 98 **2.1 Experimental design**

99 The mid-Holocene (MH) time-slice climate experiment (6000 years BP) represents the initial state for  
100 the last 6000 years transient simulation with dynamical vegetation. It is thus considered as a reference climate in  
101 this study. Because of this, and to save computing time, model adjustments made to set up the model content and  
102 the model configuration were mainly done running MH and not pre-industrial (PI) simulations (Table 1 and 2).  
103 Only a subset of PI simulation is available for comparison with modern conditions. All the simulations were run  
104 long enough (300-1000 years) to reach a radiative equilibrium and be representative of a stabilized MH climate  
105 (Fig. 1). They are free of any artificial long term trends after the adjustment phase, as were IPSL PMIP3 MH  
106 simulations (Fig. 1, Kageyama et al., 2013a).

107 Most tests follow the MH PMIP3 protocol (Braconnot et al., 2012). This is only due to the fact that this  
108 work began before the PMIP4 boundary conditions were available. But the transient simulation (TRHOLV, for  
109 TRansient HOlocene simulation with dynamical Vegetation), and the 1000 year-long MH simulations with or  
110 without dynamical vegetation that were run to prepare the initial state for it, follows the PMIP4-CMIP6 protocol  
111 (Otto-Bliesner et al., 2017, Tab. 1). In all simulations the Earth's orbital parameters are derived from Berger  
112 (1978). The MH PMIP3 protocol uses the trace gases (CO<sub>2</sub>, CH<sub>4</sub> and N<sub>2</sub>O) reconstruction from ice core data by  
113 Joos and Spahni (2008). It has been updated for PMIP4, using new data and a revised chronology that provides  
114 a consistent history of the evolution of these gases across the Holocene (Otto-Bliesner et al., 2017). The

115 difference in forcing between PMIP4 and PMIP3 was estimated to be  $-0.8 \text{ W.m}^{-2}$  by Otto-Bliesner et al. (2017).  
116 This is the order of magnitude found for the imbalance in net surface heat flux at the beginning of the MH-  
117 FPMIP4 simulation. This simulation started from L11Aer run with PMIP3 protocol (Fig. 1a). It uses the same  
118 model version, but follows the PMIP4 protocol. For the subset of PI experiments Earth's orbit and trace gases  
119 are prescribed to year 1860, i.e. the beginning of the industrial area. For the MH and PI time slice experiments,  
120 boundary conditions do not vary with time. For the transient simulations the Earth's orbital parameters and trace  
121 gases are updated every year.

122 In standard versions of the IPSL model, aerosols are accounted for by prescribing the optical  
123 distribution of dust, sea-salt, sulfate and particulate organic matter (POM), so as to take into account the  
124 coupling between aerosols and radiation (Dufresne et al., 2013). For MH simulations these variables are  
125 prescribed to 1860 CE values, for which the level of sulfate and POM is slightly higher than the values found in  
126 the Holocene (Kageyama et al., 2013a). Here, except for the first few tests (Tab. 1), we prescribe only dust and  
127 sea-salt to their 1860 values and neglect the other aerosols. A fully coupled dust-sea salt-climate version of the  
128 model that does not consider the other aerosols is under development for long transient simulations. For future  
129 comparisons it is important to have similar model set up. Indeed, compared to the version with all aerosols,  
130 considering only dust and sea salts imposes a radiative difference of about  $2.5 \text{ W.m}^{-2}$  in external climate forcing.  
131 Its footprint appears on the net heat flux imbalance at the beginning of L11Aer. It leads to a global air  
132 temperature increase of  $1.5 \text{ }^\circ\text{C}$  (Fig. 1c). The largest warming over land is found in the northern hemisphere, but  
133 the ocean warms almost everywhere by about  $1^\circ\text{C}$ , except in the Antarctic circumpolar current (Fig. 2a). The  
134 warmer conditions favor higher precipitation with a global pattern rather similar to what is found in future  
135 climate projections (Fig. 2b). This offset affects the mean climate state and is larger than the expected effect of  
136 Holocene dusts.

## 137 2.2 The IPSL Earth System Model and updated version of the land surface scheme

138 For these simulations, we use a modified version of the IPSLCM5A model (Dufresne et al., 2013). This  
139 model version couples the LMDZ.4 atmospheric model with  $144 \times 142$  grid points in latitude and longitude  
140 ( $2.5^\circ \times 1.27^\circ$ ) and 39 vertical levels (Hourdin et al., 2013) to the ORCA2 ocean model at  $2^\circ$  resolution (Madec,  
141 2008). The ocean grid is such that resolution is enhanced around the equator and in the Arctic due to the grid  
142 stretching and pole shifting. The LIM2 sea-ice model is embedded in the ocean model to represent sea ice  
143 dynamics and thermodynamics (Fichefet and Maqueda, 1999). The ocean biogeochemical model PISCES is also  
144 coupled to the ocean physics and dynamics to represent the marine biochemistry and the carbon cycle (Aumont  
145 and Bopp, 2006). The atmosphere-surface turbulent fluxes are computed taking into account fractional land-sea  
146 area in each atmospheric model grid box. The sea fraction in each atmospheric grid box is imposed by the  
147 projection of the land-sea mask of the ocean model on the atmospheric grid, allowing for a perfect conservation  
148 of energy (Marti et al., 2010). Ocean-sea-ice and atmosphere are coupled once a day through the OASIS coupler  
149 (Valcke, 2006). All the simulations keep exactly the same set of adjusted parameters as in Dufresne et al. (2013)  
150 for the ocean-atmosphere system.

151 The land surface scheme is the ORCHIDEE model (Krinner et al., 2005). It is coupled to the  
152 atmosphere at each atmospheric model 30 min physical time steps and includes a river runoff scheme to route  
153 runoff to the river mouths or to coastal areas (d'Orgeval et al., 2008). Over the ice sheet water is also routed to



154 the ocean and distributed over wide areas so as to mimic iceberg melting and to close the water budget (Marti et  
155 al., 2010). This model accounts for a mosaic vegetation representation in each grid box, considering 13  
156 (including 2 crops) plant functional types (PFT) and interactive carbon cycle (Krinner et al., 2005).

157 We made several changes in the land-surface model (Tab. 1). The first one concerns the inclusion of the  
158 11 layer physically-based hydrological scheme (de Rosnay et al., 2002) that replaces the 2 layer bucket-type  
159 hydrology (Ducoudré et al., 1993). The 11 layer hydrological model had never been tested in the full coupled  
160 mode before this study. We gave specific care to the closure of the water budget of the land surface model to  
161 ensure that  $O(1000)$  years simulations will not exhibit spurious drift in sea level and salinity. In addition the new  
162 prognostic snow model was included (Wang et al., 2013). The scheme describes snow with 3 layers that are  
163 distributed so that the diurnal cycle and the interaction between snowmelt and runoff are properly represented. In  
164 order to avoid snow accumulation on a few grid points, snow depth is not allowed to exceed 3m. The excess  
165 snow is melted and added to soil moisture and runoff while conserving water and energy (Charbit and Dumas,  
166 pers. communication). Because of a large cold bias in high latitudes in the first tests, we reduced the bare soil  
167 albedo that is used to combine fresh snow and vegetation in the snow aging parameterization. Other changes  
168 concern the adjustments of some of the parameterizations. The way the mosaic vegetation is constructed in  
169 ORCHIDEE favors too much bare soil when leaf area index (LAI) is low (Guimberteau et al., 2018). To  
170 overcome this problem, an artificial 0.70 factor was implemented in front of bare soil evaporation to reduce it  
171 (Table. 1). This factor is compatible with the order of magnitude of the reduction brought by the implementation  
172 of a new evaporation parametrization for bare soil in the current IPSLCM6A version of the model (Peylin pers.  
173 communication.). For all the other surface types the evaporation is computed as in L11. The last adjustment  
174 concerns the combination of snow albedo with the vegetation albedo. The procedure was different when  
175 vegetation was interactive or prescribed. Now, the combination of snow and vegetation albedo is based on the  
176 effective vegetation cover in the grid box in both cases. It leads to larger albedo than with the IPSL-CM5A-LR  
177 reference version when vegetation is prescribed. It counteracts the effect of the fresh snow albedo reduction.

### 178 2.3 Impact of the different changes on model climatology and performances

179 Figure 1 and 2 highlight how the changes discussed in section 2.2 affect the model adjustment and  
180 climatology. The hydrological model (L11) produces about  $1.25 \text{ mm.d}^{-1}$  higher global annual mean evaporative  
181 rates than MH PMIP3. The water cycle is more active in L11. Precipitation is enhanced in the mid-latitudes and  
182 over the tropical lands (Fig. 2c) where larger evapotranspiration and cloud cover both contribute to cool the land  
183 surface (Fig. 2d). A higher evaporative rate should lead to a colder global mean temperature (Fig. 1c). This is not  
184 the case. The large scale cooling over land is compensated by warming over the ocean (Fig. 2d), caused by  
185 reduced ocean evaporation and changes in the ocean-land heat transport. The radiative equilibrium is achieved at  
186 the top of the atmosphere with the same global mean long wave and short wave radiation budget in the two  
187 simulations (L11 and MH-PI). The effect on precipitation is larger than the one due to the aerosol forcing  
188 discussed in section 2.1. The aerosol forcing induces mainly local thermodynamic changes. The effect of the L11  
189 hydrology on evaporation induces larger changes in atmospheric circulation and thereby on precipitation.

190 The factor introduced to reduce bare soil evaporation didn't lead to the expected reduction of  
191 evaporation (Fig 1b). Indeed, when evaporation is reduced, soil temperature increases and the regional climate  
192 gets warmer allowing for more moisture in the atmosphere and thereby more evaporation where soil can supply

193 water (Fig. 2 e and f and Fig. 1). Therefore, differences resulting from bare soil evaporation do not show up on  
194 the precipitation map (Fig. 2 e) but on the increased temperature over land in the northern hemisphere (Fig. 1f).  
195 It is consistent with similar findings when analyzing land use feedback (Boisier et al., 2012). This stresses once  
196 more that fast feedbacks occur in coupled systems and that any comparison of surface fluxes should consider  
197 both the flux itself and the climate or atmospheric variables used to compute it (Torres et al., 2018). Note that in  
198 figure 2 f about 0.1°C of the 0.4°C global warming in L11AerEv is still a footprint of the warming induced by  
199 the aerosol effect described in section 2.1, but that it doesn't alter our conclusions on the regional temperature-  
200 evaporation feedback.

201 The difference between MH-FPMIP4 and MH-PMIP3 represents the sum of all the changes in the land  
202 surface model and forcing discussed above (Fig. 2 g and h). A PI simulation performed with the new model  
203 version (PI-FPMIP4, Tab. 1) allows us to assess how they affect the model performances. A rapid overview of  
204 model performances is provided by a simple set of metrics derived from the PCMDI Metric Package (Gleckler et  
205 al., 2016, see appendix 1). Figure 3 highlights that temperature biases are reduced in PI-PMIP4 at about all  
206 model levels but that biases are enhanced for precipitation and total precipitable water compared to PI-PMIP3  
207 (comparison of blue and black lines in Fig. 3). Taken all together all the changes we made have little effect on  
208 the bias pattern (Fig. 3a). The model performs quite well compared to the CMIP5 ensemble of PI simulations,  
209 except for cloud radiative effect (Fig. 3). The effect of cloud in the IPSLCM5A-LR simulations has already been  
210 pointed out in several manuscripts and results mainly from low level clouds over the ocean (Braconnot and  
211 Kageyama, 2015; Vial et al., 2013). The atmospheric tuning is exactly the same as in the default IPSLCM5A-LR  
212 version, and the introduction of all the changes described above have almost no effect on the cloud radiative  
213 effect. Overall the model version with the 11 layer hydrology has similar skill as the IPSLCM5A reference  
214 (Dufresne et al., 2013) and we are confident that the version is sufficiently realistic to serve as a basis on top of  
215 which we can include the dynamical vegetation.

#### 216 **2.4 Initialization of the mid-Holocene dynamical vegetation for the transient simulation**

217 We added the vegetation dynamics by switching on the dynamical vegetation model described in Zhu et  
218 al. (2015). Compared to the original scheme (Krinner et al., 2005), it produces more realistic vegetation  
219 distribution in mid and high latitude regions when compared with present-day observations.

220 Two different strategies have been tested to initialize the dynamical vegetation (Table 2). In the first  
221 case (MH-Vmap), the initial vegetation distribution was obtained from an off line simulation with the land  
222 surface model forced by CRU-NCEP 1901-1910 climatology. In the second case (MH-Vnone), the model  
223 restarted from bare soil with the dynamical vegetation switched on, using the same initial state as MH-Vmap for  
224 the atmosphere, the ocean, the sea-ice and the land-ice. As expected, the evolution of baresoil, grass and tree is  
225 very different between MH-Vmap and MH-Vnone during the first adjustment phase (black and blue curves in  
226 Fig. 4 a,b, and c). Vegetation adjusts in less than 100 years (1200 months) in MH-Vmap (blue curve). This short  
227 term adjustment indicates that the climate-vegetation feedback has a limited impact on vegetation when the  
228 initial state is already consistent with the characteristics of the simulated climate. In MH-Vnone that starts from  
229 baresoil (black curve), the adjustment has a first rapid phase of 50 years for bare soil and about 100 years for  
230 grass and tree, followed by a longer phase of about 200 years. The latter corresponds to a long term oscillation  
231 that has been induced by the initial coupling choc between climate and land surface. Note that PMIP4 instead of

232 PMIP3 MH boundary conditions were used to run the last part of these simulations (red and yellow curves in  
233 Fig. 4 a, b, and c). In the coupled system, most of the vegetation adjustment takes about 300 years, which is  
234 longer than results of off line ORCHDEE simulations (less than 200 years). Since MH-Vnone started from a  
235 coupled ocean-atmosphere-ice state at equilibrium, this result also indicates that the land-sea-atmosphere  
236 interactions do not alter much the global energetics of the IPSL model in this simulation where atmospheric CO<sub>2</sub>  
237 is prescribed. The two simulations converge to very similar global vegetation cover. Figure 4 suggests that there  
238 is only one global mean stable state for the mid-Holocene with the IPSL model, irrespective of the initial  
239 vegetation distribution (see also Tab. A2, appendix A2).

240 For the transient simulations, we decided to use the results of the MH-VNone simulation as initial state  
241 (Table 2). We performed a preindustrial simulation (PI-Vnone) using MH-Vnone as initial state and switching  
242 on the orbital parameters and trace gases to their PI values. Figure 3 indicate that the vegetation feedback slightly  
243 degrades the global performances for PI temperature and bring the model performance close to the IPSLCM5A-  
244 LR CMIP5 version. It also contributes to reduce the mean bias in precipitable water, evaporation, precipitation  
245 and long wave radiation, but it has no effect on the bias pattern (assessed by the rmst in Fig. 3, see also  
246 appendix). Vegetation has thus an impact on climate, but this effect is smaller than those done to set up the  
247 model version we use here. Section 4 provides a more in depth discussion on vegetation state.

## 248 3 Simulated climate and vegetation throughout the mid to late Holocene

### 249 3.1 Long term forcing

250 Starting from the MH-Vnone simulation the transient simulation of the last 6000 years (TRHOLV)  
251 allows us to test the response of climate and vegetation to atmospheric trace gases and Earth's orbit (see section  
252 2.1). The atmospheric CO<sub>2</sub> concentration is slowly rising throughout the Holocene from 264 ppm 6000 years ago  
253 to 280 for the pre-industrial climate around -100 BP (1850 CE) and then experiences a rapid increase from -100  
254 BP to 0 BP (1950 CE) (Fig. 5). The methane curve shows a slight decrease and then follows the same evolution  
255 as CO<sub>2</sub>, whereas NO<sub>2</sub> remains around 290 ppb throughout the period. The radiative forcing of these trace gases is  
256 small over most of the Holocene (Joos and Spahni, 2008). The largest changes occurred with the industrial  
257 revolution. The rapid increase in the last 100 years of the simulation has an imprint of about 1.28 W.m<sup>-2</sup>.

258 The major forcing is caused by the slow variations of the Earth's orbital parameters that induce a long  
259 term evolution of the magnitude of the incoming solar radiation seasonal cycle at the top of the atmosphere (Fig.  
260 5). It corresponds to decreasing seasonality in the northern Hemisphere and increasing seasonality in the  
261 southern Hemisphere (Fig. 5). It results from the combination of the changes in summer and winter insolation in  
262 both hemispheres (Fig. 6). These seasonal changes are larger at the beginning of the Holocene (about -8 W.m<sup>-2</sup>  
263 per millennia in the NH and +5 W.m<sup>-2</sup> per millennia in the SH) and then the rate of change linearly decreases in  
264 the NH (increases in the SH) from 4500 to about 1000 years BP. There is almost no change in seasonality in the  
265 NH over the last 1000 years, whereas in the SH seasonality starts to decrease again by 2000 years BP. The shape  
266 of insolation changes is thus different in both hemisphere, and so is the relative magnitude of the seasonal cycle  
267 between the two hemispheres. This would be seen whatever the calendar we use to compute the month means  
268 because of the seasonal asymmetry induced by precession at the MH (see: Joussaume and Braconnot, 1997;  
269 Otto-Bliesner et al., 2017).

### 270 3.2 Long term climatic trends

271 Changes in temperature and precipitation follow the long term insolation changes in each hemisphere  
272 and for the different seasons until about 2000 yrs BP to 1500 yrs BP (Fig. 6). Then trace gases and insolation  
273 forcing become equivalent in magnitude and small compared to MH insolation forcing, until the last period  
274 where trace gases lead to a rapid warming. The NH summer cooling reaches about 0.8 °C and is achieved in  
275 4000 years. The last 100 year warming reaches 0.6 °C and almost counteracts, for this hemisphere and season,  
276 the insolation cooling. SH summer (JJAS) and NH Winter conditions (NDJF) are both characterized by a first  
277 2000 years warming induced by insolation. It reaches about 0.4°C. It is followed by a plateau of about 3000  
278 years before the last rapid increase of about 0.6°C that reinforces the effect of the Holocene insolation forcing.  
279 During SH winter temperature does not seem to be driven by the insolation forcing (Fig. 6 d). In both  
280 hemispheres summer precipitation trends correlate well to temperature trends, as it is expected from a  
281 hemispheric first order response driven by Clausius Clapeyron relationship (Held and Soden, 2006). This is not  
282 the case for winter conditions because one needs to take into account the changes in the large scale circulation  
283 that redistribute heat and energy between regions and hemispheres (Braconnot et al., 1997; Saint-Lu et al., 2016).  
284 We further estimate the linkages between the long term climate response and the insolation forcing for  
285 the different latitudinal bands by projecting the zonal mean temperature and precipitation seasonal evolution on  
286 the seasonal evolution of insolation. We define the seasonal amplitude for each year as the difference between  
287 the maximum and minimum monthly values. We consider for each latitude the unit vector  $\mathbf{S}$ :

$$288 \mathbf{S} = \frac{\mathbf{SW}_{is-TOA}}{\|\mathbf{SW}_{is-TOA}\|} \quad (1),$$

289 where  $\|\mathbf{SW}_{is-TOA}\|$  represents the norm of the seasonal magnitude of the incoming solar radiation at TOA over  
290 all time steps ( $\mathbf{SW}_{is-TOA}(t)$ ,  $t=-6000$  years to 0, with an annual time step). Any climatic variable ( $\mathbf{V}$ ) can then be  
291 expressed as:

$$292 \mathbf{V}(t) = \alpha(t)\mathbf{S} + \beta(t)\mathbf{b} \quad (2),$$

293 with:

$$294 \alpha = \mathbf{V} \cdot \mathbf{S} \quad (3),$$

295 and  $\mathbf{b}$  is the unit vector orthogonal to  $\mathbf{S}$ . The ratio  $\alpha/(\alpha + \beta)^2$  measure in which proportion a signal projects on  
296 the insolation (Figure 7). Figure 7 confirms that the projection of temperature and precipitation on the insolation  
297 curve is larger in the northern than in the southern hemisphere. The best match is obtained between 10°N and  
298 40°N where about 80 % of the temperature signal is a direct response to the insolation forcing. The projections  
299 are only 40% in the tropics in the southern hemisphere. These numbers go up to 90% if a 100 year smoothing is  
300 applied to temperature. The seasonality precipitations project also to 90% when considering the filtered signal,  
301 confirming the strong linkages between temperature and precipitation in the NH over the long time scale. The  
302 projection is poorer, but not null, when the raw precipitation signal is considered. At the equator and in high  
303 latitudes in both hemispheres the projection is poor or null. At the equator, the MH insolation forcing favours a  
304 larger north/south seasonal march of the ITCZ over the ocean and the inland penetration of AfroAsian monsoon  
305 precipitation during boreal summer. Surface temperature is reduced in regions where precipitation is enhanced  
306 due to the combination of increased cloud cover and increased surface evaporation (Braconnot et al., 2007a;  
307 Joussaume et al., 1999). When monsoon retreats to its modern position, surface temperature in these regions  
308 increases, thereby enhancing its seasonal cycle. It is thus out of phase compared to the insolation forcing. This is

306 also true over SH continents where temperatures in regions affected by monsoons do not follow the local  
307 insolation and has similar seasonal evolution than the northern hemisphere. This out of phase relationship is  
308 consistent with glaciers reconstructions (Jomelli et al., 2011). In higher latitude the projection of the raw signal  
309 does not project well because of the large decadal variability. North of 40°N the mixed layer depth is also larger  
310 (about 200 m) than in the tropics (about 70m), which contribute to damp the seasonal change over the ocean.  
311 Thereby the seasonal temperature response is flatter than the shape of the seasonal insolation forcing, which lead  
312 to a poor projection over mid and high latitudes ocean especially in the ocean dominated SH (Fig. 7). Sea ice  
313 cover has also little change north of 80°N which also damps the changes in seasonality (Fig. 8). These changes  
314 are however amplified by the increase of sea ice during summer in the Arctic resulting from cooler conditions  
315 with time, and by the reduction of the winter sea-ice cover in the Labrador and the Gin seas (Fig. 8a and b). For  
316 the snow cover the conditions are contrasted depending on the regions (Figure 8 b and d), with an increase  
317 decrease of the maximum cover over Eurasia related to long term rise of minimum temperature (Fig. 8 d)

### 318 3.3 Long term vegetation trends

319 These long term climate evolutions have a counterpart on the long term evolution of vegetation (Fig. 9).  
320 At the global and hemispheric scale, the long term vegetation trends correspond to reductions or increases of the  
321 area covered by vegetation reaching 2 to 4% of the total land area depending on vegetation type (Fig. 9). The  
322 global vegetation averages reflect the northern hemisphere changes where most of the vegetated continental  
323 masses are located. As expected from the different long term trend in insolation, the long term evolution of tree  
324 and grass covers are opposite between the two hemispheres. Note however that bare soil slightly increases in  
325 both hemispheres.

326 In the northern hemisphere the changes follow the changes in summer temperature, with the best match  
327 obtained for grass which increases almost linearly until 2000 years BP and then remains quite stable. In the  
328 southern hemisphere the phasing between vegetation change and temperature is not as good, again because this  
329 hemisphere is dominated by ocean conditions rather than land conditions. However, the tree expansion reaches a  
330 maximum between 2000 year BP and 1000 years BP and then the tree cover slightly decreases, which  
331 corresponds to the slight cooling in SH summer temperature. The gross primary productivity (GPP, Fig. 9 d) is  
332 driven in both hemispheres by the changes in tree cover. It accounts for a reduction of about 5 PgCy<sup>-1</sup>. It is  
333 however possible that the GPP change is misestimated in this simulation because CO<sub>2</sub> is prescribed in the  
334 atmosphere, which implies that the carbon cycle is not fully interactive. Figure 10 compares the vegetation map  
335 obtained for the pre-industrial period in TRHOLV (50 years around 1850 AC, which corresponds to 150 - 100  
336 years BP) with MH vegetation. It shows that bare soil increases in semi-arid regions in Africa and Asia, as well  
337 as in South Africa and Australia. The reduction in tree PFTs is maximum north of 60°N, in South and Southeast  
338 Asia, Sahel and most of North America. They are replaced by grass PFTs. In the southern hemisphere forest  
339 cover increases in South Africa, South East South America and part of Australia.

340 In the last 100 years the effect of trace gases and in particular the rapid increase of the atmospheric CO<sub>2</sub>  
341 concentration leads to a rapid vegetation change characterized by tree regrowth, which is dominant in the NH  
342 (Fig. 9 and 10). This tree recovery counteracts the reduction from mid Holocene in mid and high NH latitudes  
343 (Fig. 10 b, e, and h). This effect is consistent with the observed historical growth in gross primary production  
344 discussed by Campbell et al. (2017). The GPP increase in the last 100 years results from increased atmospheric

345 CO<sub>2</sub>. It suggests that the CO<sub>2</sub> effect counteracts the tree decline induced by insolation. When reaching 0k BP  
346 (1950 CE), bare soil remains close to PI, grass reduces by 3% and tree increases by about 3%.

### 347 3.4 Regional trends

348 Figure 11 highlights the long term vegetation trends for three regions that respectively represent climate  
349 conditions north of 60°N, over the Eurasian continent, and in the West African monsoon Sahel/Sahara region.  
350 These are regions for which there are large differences in MH – PI climate and vegetation cover (Fig. 9 and 10).  
351 They have also been chosen because they are widely discussed in the literature and are also considered as tipping  
352 points for future climate change (Lenton et al., 2008). They are well suited to provide an idea of different  
353 characteristics between regions.

354 North of 60°N and in Eurasia a substantial reduction of tree at the expense of grass starts at 5000 years  
355 BP (Fig. 11 a and b). Vegetation has almost its pre-industrial conditions around 2500 years BP. The largest  
356 trends are found between 5000 years BP and 2500 years BP in this region and this reflects well the timing of the  
357 NH hemisphere summer cooling. The change in total forest in Eurasia is small. A first change is followed by a  
358 second one around 3000 years BP. Despite the 100 year smoothing applied to all the curves, they exhibit large  
359 decadal to multi-centennial variability. Over West Africa (Fig. 11c), the largest trends start slightly later (4500-  
360 5000 years BP) and are more gradual until 500 years BP. The vegetation trends are also punctuated by several  
361 centennial events that do not alter much the long term evolution as some of these events do in the other two  
362 boxes.

363 The variability found for vegetation is also found in temperature and precipitation at the hemispheric  
364 scale (Fig. 6). It is even higher at the regional scale in mid and high latitudes (Fig 8). This variability is not  
365 present in the imposed forcing. It results from internal noise. Because of this it is difficult for example to say if  
366 the NH hemisphere winter temperature trend was rapid until 4000 years BP and then temperature remains stable,  
367 or if the event impacting temperature and precipitation around 4800 to 4500 BP masks a more gradual increase  
368 until 3000 BP as it is the case for NH Summer where the magnitude of the temperature trend is larger than  
369 variability (Fig. 6). Note that some of these internal fluctuations reach half of the total amplitude of the regional  
370 vegetation trends (Fig. 11), and that it is a dominant signal over Eurasia, where the long term mean change in the  
371 total tree cover is small (Fig. 10 and 11). Temperature and precipitation are well correlated at this centennial  
372 time scale (Fig. 6).

373 Despite the dry bias over the Sahel region in this version of the model, the timing of the vegetation  
374 changes over West Africa reported in figure 11 is consistent with the major features discussed for the end of the  
375 African humid period (Hély and Lézine, 2014; Liu et al., 2007). In particular, the replacement of grass by bare  
376 soil starts earlier than the reduction of the tree cover located further south (Fig. 11). At the scale of the Sahel  
377 region, we do not have abrupt but gradual changes in vegetation. It is however abrupt at the grid cell level. These  
378 changes are associated with the long term decline of precipitation, as well as the southward shift of the tropical  
379 rain belt associated with the African monsoon (Fig. 12). The location (latitude) of the rain belt is estimated here  
380 as the location of the maximum summer precipitation zonally averaged between 10°W and 20°E over West  
381 Africa. Most of the southward shift of the rain belt occurs between MH and 3500 years BP and correspond to a  
382 difference of about 1.8°N of latitude over this period. Then the southward shift is smaller, with a total shift of  
383 2.5°N of latitude diagnosed in this simulation. The comparison of figure 11 and 12 clearly shows that the rapid

384 decrease of vegetation occurs after the rapid southward shift of the rain belt. An interesting point is that the  
385 amount of precipitation is also shifted in time compared to the location of the rain belt. It suggests that the  
386 vegetation feedback on precipitation is still effective during the first period of precipitation decline and that it  
387 might have amplify the reduction of precipitation when vegetation is reduced over the Sahel region.

388 As seen in figure 10, the NH decrease in forest cover is mainly driven by the changes that occur north of  
389 60°N (Fig. 8 and 10). These trends reflect more or less what is expected from observations (Bigelow et al., 2003;  
390 Jansen et al., 2007; Wanner et al., 2008). It results from the summer cooling that affects both the summer sea-ice  
391 cover in the Arctic, the summer snow cover over the adjacent continent and the amplification of the insolation  
392 forcing south of 70°N by snow/vegetation albedo feedback. Further south over Eurasia, figure 11 suggests that  
393 there are only marginal changes in Eurasia in terms of vegetation. Figure 13 shows the total tree cover over this  
394 region does not reflect well the mosaic vegetation and forest composition. Indeed, the long term decrease in  
395 forest is dominated by the decrease in temperate and boreal deciduous trees. Boreal needle leaf evergreen trees  
396 do not change whereas the temperate ones increase. This figure also highlights that the long term change in  
397 Eurasian tree composition throughout the mid to late Holocene is punctuated by centennial variability. The  
398 different trees have also different timing and variability. Boreal forests are more sensitive to variability during  
399 the first 3000 years of the simulation, whereas, temperate broadleaf tree exhibit larger variability in the second  
400 half. The large events have a climatic counterpart (Fig. 8), so that the composition of the vegetation is a result of  
401 a combined response to the long term climatic change and to variability. These two effects can lead to different  
402 vegetation composition depending on stable or unstable vegetation states (Scheffer et al., 2012). Decadal  
403 vegetation changes have been discussed for recent climate in these regions (Abis and Brovkin, 2017), which  
404 suggests that despite the fact that our dynamical vegetation model might underestimate vegetation resilience, the  
405 rapid changes in vegetation mosaic is a key signal over Eurasia. Future model data comparisons should consider  
406 composition changes and variability to properly discuss vegetation changes over this region.

## 407 **4 Vegetation, uncertainties and multiple vegetation states**

### 408 **4.1 Simulated versus reconstructed vegetation**

409 Section 3 shows how climate and vegetation respond to insolation and trace gases. The simulated  
410 changes are in broad agreement with what is expected from various sources of data. However, section 2  
411 mentions model adjustments and biases. They all contribute to the difficulty to produce the right vegetation  
412 changes at the right place, at the right time and for the right reasons. It is thus important to fully understand what  
413 we can expect in terms of realism from this simulation. We investigate it for the mid-Holocene and modern  
414 climate for which we can use the BIOME6000 vegetation reconstruction (Harrison, 2017).

415 The dynamical vegetation module simulates fractional cover of 13 PFTs. These PFTs cannot be directly  
416 compared with the reconstructed biome types based on pollen and plant macrofossil data from the BIOME 6000  
417 dataset (Harrison, 2017). In order to facilitate the comparison, we converted the simulated PFTs into eight mega-  
418 biomes, using the biomization method algorithm proposed by Prentice et al. (2011). The algorithm uses a  
419 mixture of simulated climate and vegetation characteristics (see appendix and Fig. A2). Alternative thresholds as  
420 proposed in previous studies (Joos et al., 2004; Prentice et al., 2011) were tested to account for the uncertainties  
421 in the biomization method (see Fig. A2). At first look MH-Vnone reproduces the large scale pattern found in the

422 BIOME6000 reconstruction (Fig. 14a). The comparison however indicates that the boreal forest tree line is  
423 located too far south. It results from a combination of a cold bias in temperature in these regions and a systematic  
424 underestimation of forest biomass in Siberia with ORCHIDEE when forced by observed present-day climate  
425 (Guimberteau et al., 2018). Such underestimation of tree biomass could lead to too low tree height in  
426 ORCHIDEE, and thus to the replacement of boreal forest by dry woodland according to the biomization  
427 algorithm (Fig. A2a). Also, vegetation is underestimated in West Africa, consistent with a dry bias (not shown).  
428 The underestimation of the African monsoon precipitation is present in several simulations with the IPSL model  
429 (Braconnot and Kageyama, 2015), and is slightly enhanced in summer when the dynamical vegetation is active.  
430 With interactive vegetation however equatorial Africa is more humid (Fig. 15a). Figure 14c provides an idea of  
431 the major mismatches between simulated vegetation and the BIOME6000 reconstructions. In particular the  
432 simulation produces too much desert where we should find grass and shrub. It also produces too much tundra  
433 instead of boreal forest, and too much savanah and dry woodland in several places that should be covered by  
434 temperate-tree, boreal-tree or tundra, confirming the visual map comparison (Fig. 14c). Similar results are found  
435 when considering the pre-industrial climate in TRHOLV compared to the BIOME6000 pre-industrial biome  
436 reconstruction (see Fig. A2 d). These are systematic biases. These systematic biases are confirmed when  
437 comparing the simulated PFTs for PI with those of the 1860 PI map estimated from observations and used in  
438 simulations with prescribed vegetation (see Tab. A2 for regions without land use).

439 It is not possible to estimate the vegetation feedback on the long term climate evolution from the  
440 transient simulation. It is however possible to infer how the dynamical vegetation affects the mean climatology  
441 for the MH, period for which simulations with prescribed and dynamic vegetation are available. Metrics  
442 discussed in section 2.4 (Fig. 3) show that the introduction of the dynamical vegetation in the model reduces the  
443 amount of precipitation and that the climate is dryer. The simulations with dynamical vegetation only consider  
444 natural vegetation, whereas the 1860 map we prescribe when vegetation is fixed include land use. In regions  
445 affected by land use all MH simulations produce less baresoil (3%), more tropical trees (5%), similar temperate  
446 tree cover, increased boreal tree cover (10%) and a different distribution between C3 versus C4 grass (see Tab.  
447 A2). In Eurasia where croplands are replaced by forest, the lower forest albedo induces warmer surface  
448 conditions (Figure 15 b). Also, when snow combines with forest instead of grasses, the snow/vegetation albedo  
449 is lower leading to the positive snow-forest feedback widely discussed for the last glacial inception (de Noblet et  
450 al., 1996; Kutzbach et al., 1996). Figure 15a also highlights that precipitation is increased over the African  
451 tropical forest and reduced over South America. In most regions the impact of vegetation is much smaller than  
452 the impact of the changes in the land surface hydrology and forcing strategy discussed in sections 2.3 (Fig. 2).

453 The differences between the MH simulated vegetation map and the 1860 PI map reflect both systematic  
454 model biases and vegetation changes related to the MH climate differences with PI. We can infer from figures 15  
455 and 16 that vegetation has a positive warming feedback in the high latitudes during MH. Part of the differences  
456 between the MH and the PI conditions in figure 15 c and d are dominated by the impact of vegetation. Similar  
457 patterns as those obtained for the impact of vegetation are found over Eurasia for temperature, or south East Asia  
458 and North America for precipitation. For the grid points where BIOME6000 data are available for both MH and PI  
459 (0k), the major simulated biome changes occur for Savana&Wood and Grass &Shrub (Fig. 14 e). Differences are  
460 also found for tree and tundra, to a lesser extent. The comparison with similar estimates from BIOME6000  
461 reconstructions indicates that Grass &shrub exhibit the major changes and that tree show larger differences



462 compared to the simulation. The model shift between Savana&Wood and Grass &shrub is consistent with the  
463 noted bias for Savana and the fact that the tree cover is underestimated in norther NH latitudes (Fig. 14).

464 Note that the vegetation differences found between the historical period and the PI period in TRHOLV  
465 are not negligible. We can estimate from figure 15 a and b that neglecting land use leads to an underestimation of  
466 about 1°C in Eurasia between the MH and PI in this TRHOLV simulation. Depending if PI or the historical  
467 period is used as reference the magnitude of the MH changes in vegetation and climate would be different. Also  
468 land use has regional impacts and should be considered in PI or in the historical period. This stresses that  
469 quantitative model-data comparison should be considered with care, knowing that both the reference period (PI  
470 or historical) and the complexity of the land surface model (prescribed vegetation, natural dynamical vegetation,  
471 land use...) can easily lead to 1°C difference in some regions.

472

## 473 4.2 Multiple vegetation states for the pre-industrial climate

474 Another source of uncertainty concerns the stability of the simulated vegetation maps. Several studies  
475 suggest that the initial state has only minor impact on the final climate because there is almost no changes in the  
476 thermohaline circulation over this period and models do not exhibit major climate bifurcations (e.g. Bathiany et  
477 al., 2012). This is the main argument used by Singarayer et al. (2010) to justify that their suite of snap shot  
478 experiments may provide reasonable transient climate vision when put together. Is it the case in the TRHOLV  
479 simulation when vegetation is fully interactive? This transient simulation does not exhibit much change in  
480 indices of thermohaline circulation that remains close to 16-18 Sv ( $1 \text{ Sv} = 10^6 \text{ m}^3 \cdot \text{s}^{-1}$ ) throughout the period. The  
481 global metrics (Fig. 3) show that at the global scale the results of the TRHOLV simulations for PI (around 100  
482 BP = 1860 AC) are similar to those of PI-Vnone. It is also the case for seasonal and extratropical/tropical values  
483 (Fig. A1). We can therefore conclude that there is no difference in mean surface climate characteristics between  
484 the snap shot PI-Vnone experiments and the PI period simulated in transient TRHOLV simulation.

485 Then, is the vegetation also similar to the one simulated in PI-VNNone? The PI vegetation simulated in  
486 TRHOLV shows little differences to the one found for PI-Vnone (Fig. 10 c, f, and i). The relative percentages of  
487 land covered by the different vegetation classes correspond to 15% for bare soil, 41% for grass and 43% for tree  
488 respectively. These values are similar to the one found for PI-VNNone (15%, 40% and 44% respectively) within  
489 1% error bar. This doesn't necessarily hold at the regional scale where regional differences are also found  
490 between PI-THROLV and PI-Vnone. Indeed, figure 10 indicates differences in tree and grass cover in Eurasia  
491 around 60°N and different geographical coverage between bare soil, grass and trees over South Africa and  
492 Australia. These differences are very small compared to the differences between MH and PI in TRHOLV, but  
493 are as large as the difference between hist and PI in a few places in Eurasia. As seen in previous section, these  
494 are regions where variability is large and vegetation instable.

495 We also tested if the PI vegetation and climate would also be similar when starting from MH-Vmap  
496 instead of MH-Vnone (dark pink and orange lines in Fig. 4d, e and f). This is also a way to have a better idea of  
497 the range of response one would expect from ensemble simulations, knowing that we only ran one full transient  
498 simulation. For the PI-Vmap simulation, the orbital parameters and trace gases were first prescribed to pre-  
499 industrial conditions for 15 years while maintaining the vegetation PFTs in each grid cell to those obtained in  
500 MH-Vmap (Tab. 2, Fig. 4). Then, the dynamical vegetation was switched on. It induces a rapid transition of the

501 major PFTs that takes about 10 years before a new global equilibrium is reached (Fig. 4 d, e and f). For PI-  
502 VNone presented in section 2.4 the same procedure was applied, but the dynamical vegetation was switched on  
503 after 5 years (Tab. 2 and Fig. 4), and the new equilibrium state is reached without any relaxation or rapid  
504 transition.

505 PI-Vnone and PI-Vmap converge to different global vegetation states (Fig. 4). Compared to the values  
506 listed above for PI-Vnone and PI-TRHOLV the respective covers of bare soil, grass and tree for PI-Vmap are  
507 20%, 37% and 43%. In particular PI-Vmap produces a larger bare soil cover than PI-Vnone (Fig. 4 d). It is even  
508 larger than the total bare soil cover found in the 1860 CE map used in PI simulations when vegetation is  
509 prescribed (Fig. 4). Interestingly part of these differences between Vmap and Vnone, are found in the southern  
510 hemisphere and the northern edge of the African and Indian monsoon regions. These differences in PI vegetation  
511 explain the vegetation differences between MH and PI (Fig. 16), and mainly concern the distribution between  
512 grass and bare soil. The simulated changes seem larger with Vmap. Previous assessment of model results against  
513 vegetation and paleoclimate reconstructions (e.g. Harrison et al., 2014; Harrison et al., 1998) suggest that MH –  
514 PI vegetation for Vmap would look in better agreement with reconstructed changes from observations in terms  
515 of forest expansion in the northern hemisphere or grasses in Sahel (Fig. 16). However, the modern vegetation  
516 map for this PI-Vmap simulation has even less forest than PI-Vnone north of 55°N (Fig. 4 e, f and i), for which  
517 forest is already underestimated (Fig. A2). These differences in PI vegetation have only a small counterpart in  
518 climate. It corresponds to cooler condition in the mid and high norther latitude (Fig. 15). In annual mean there is  
519 almost no impact on precipitation (Fig. 15). In terms of climate these two simulations are very similar, and closer  
520 to each other than to other simulations, whatever the season or the latitudinal band (see figure A1). The small  
521 differences in climate listed above are thus too small to be captured by global metrics. It suggests that there is no  
522 direct relationship between the different vegetation maps and model performances. The different vegetation  
523 maps are obtained with a similar climate, which indicates that in this model multiple global and vegetation states  
524 are possible under pre-industrial climate or that tiny climate differences can lead to different vegetation.

## 525 5 Conclusion

526 This long transient simulation over the last 6000 years with the IPSL climate model is one of the first  
527 simulations over this period with a general circulation model including a full interactive carbon cycle and  
528 dynamical vegetation. We show that, despite some model biases that are amplified by the additional degree of  
529 freedom resulting from the coupling between vegetation and climate, the model reproduces reasonably well the  
530 large scale features in climate and vegetation changes expected from the observation over this period. There has  
531 been lots of discussion on the sign of the trends in the northern mid-latitude following the results of the first  
532 coupled ocean-atmosphere simulation with the CCSM3 model across the deglaciation. Our results seem in broad  
533 agreement with the 6000 to 0 part of the revised estimates by Marsicek et al. (2018). There is little change in  
534 annual mean climate throughout the last 6000 years (not shown). The seasonal cycle is the main driver of the  
535 climate and vegetation changes, except in the last part of the simulation when the rapid greenhouse gas  
536 concentration increase leads to a rapid global warming.

537 Several points emerge from this study. The first one is that the MH-PI changes in climate and  
538 vegetation is similar in our simulation between snapshot experiments and a long transient simulation. What is the  
539 value added then of the transient simulation? The good point is that model evaluation can be done on snapshot

540 experiments, which fully validate the view that the mid-Holocene is a good period for model benchmarking in  
541 the Paleoclimate Modeling Intercomparison Project (Kageyama et al., 2018). However the MH = PI climate  
542 conditions mask the long term history and the relative timing and the rate of the changes. The major changes  
543 occur between 5000 and 2000 year BP and the exact timing depends on regions. In our simulation the forest  
544 reduction in the northern hemisphere starts earlier than the vegetation changes in Africa. It also ends earlier. The  
545 last period reflects the increase in trace gases with a rapid regrowth of tree in the last 100 years when CO<sub>2</sub> and  
546 temperature increase at a rate not seen over the last 6000 to 2000 years. Some of these results already appear in  
547 previous simulations with intermediate complexity models (Crucifix et al., 2002; Renssen et al., 2012). Using the  
548 more sophisticated model with a representation of different types of tree brings new results. Even though the  
549 total forest cover does not vary much throughout the Holocene in TRHOLV, the composition of the forest varies  
550 more substantially, with different relative timing between the different PFTs.

551 We mainly consider here surface variables that have a rapid adjustment with the external forcing. Also,  
552 we only consider long term trends in this study, but the results highlight that centennial variability plays an  
553 important role to shape the response of climate and vegetation to the Holocene external forcing at regional scale.  
554 In depth analyses of ice covered regions and of the ocean response would be needed to tell whether the  
555 characteristics of variability depends or not on the pace of climate change. It would guide the development of  
556 methodologies to assess the vegetation instabilities as the one seen in Eurasia. They might share some  
557 similarities with the vegetation variability reported in this region for the recent period (Abis and Brovkin, 2017).  
558 These simulations offers the possibility to analyze the simulated internal instability of vegetation that could be  
559 partly driven by climate noise (Alexandrov et al., 2018). The different time scales involved in this long term  
560 evolution can be seen as an interesting laboratory for further investigation in this respect.

561 The vegetation differences between PI-Vmap and PI-VNone raise once more the possibility for multiple  
562 vegetation equilibrium under pre-industrial or modern conditions as it has been widely discussed previously (e.g.  
563 Brovkin et al., 2002; Claussen, 2009). Here we have both global and regional differences. Our results are  
564 however puzzling, because we only find limited differences between the PI-Vnone snapshot simulation and the  
565 PI climate and vegetation produced at the end of TRHOLV. These simulations start from the same initial state  
566 and in one case PI condition are switch on in the forcing, whereas the other case the 6000 years long term  
567 forcing in insolation and trace gases is applied to the model. An ensemble of simulations would be needed to  
568 fully assess vegetation stability. In the northern hemisphere and over forest areas, MH-Vmap produced slightly  
569 less trees than MH-Vnone. It might have been amplified by snow albedo feedback under the PI conditions that  
570 are characterized by a colder than MH climate in high latitudes in response to reduced incoming solar radiation  
571 associated with lower obliquity. The differences between the southern and northern hemisphere characterized by  
572 large differences in grasses and bare soil are more difficult to understand and suggest different response to the  
573 changes in southern hemisphere seasonality. This is in favor of different equilibrium induced only partly by  
574 climate-vegetation feedback. We need also to raise the point that there is still a very small probability that these  
575 differences come from inconsistent modeling when vegetation is prescribed or when we use the dynamical  
576 model. This should not be the case because it would not explain why vegetation is sensitive to initial state in PI  
577 and not in MH. It is also possible that the climate instability induced by the change from one year to the other in  
578 insolation and trace gases leads to rapid amplification of climate in high latitude, which is more effective under

579 the cooling high latitude condition found in PI. The strongest conclusion from these simulations is that the  
580 vegetation-climate system is more sensitive under the pre-industrial conditions (at least in the NH latitudes).

581 This study also points out the difficulties to fully assess model results. Part of it is due to model biases  
582 that prevent the simulation to be correct at regional scale, or where data are available. Specific methodology  
583 needs to be developed for model-data comparison designed to assess the climate-vegetation dynamics over a  
584 long time scale without putting too much weight on inherent model biases. There is also an intrinsic reason  
585 related to the fact we only represent natural vegetation, and neglect land use and also aerosols other than dust  
586 and sea-salt. Therefore the PI and historical climate cannot be realistically reproduced, even though most of the  
587 characteristics we report are compatible with what has been observed. Our results also show that the assessment  
588 of the magnitude of the simulated differences between MH and modern conditions depends on the reference  
589 period. This has implication for model-data comparisons, but also for reconstruction of temperature or moisture  
590 from paleoclimate archives that are in general calibrated using specific datasets. Similar methodologies for data  
591 sampling need thus to be applied both on paleoclimate records and on model outputs. It also suggests that more  
592 needs to be done to derive criteria allowing us to assess the processes leading to the observed changes rather than  
593 the changes themselves.

## 594 6 Appendix

### 595 6.1 A1 Spatio-temporal agreement between model results and observations in the extratropics and 596 tropics

597 Figure 3 highlights the model-observation agreement for the pre-industrial climate considering global  
598 metrics, commonly used to evaluate model climatology. The mean bias ( $Bias_{xy}$ ) represents the difference  
599 between the spatio-temporal averages of a simulated variable with observations. Here all metrics consider fifty  
600 year averages from observations or reanalysis products. We estimate the spatio-temporal mean of each variable  
601 as:

$$\text{Var}_{xy} = \frac{1}{T} \sum_{i,j,t} w_{i,j} \text{Var}_{i,j,t} \quad (4)$$

602 Where  $w_{i,j}$  (with  $\sum_{i,j} w_{i,j} = 1$ ) represents the ratio of the surface of the grid-cell to the total surface of  
603 the grid, and  $T$  the number of time steps. If we call  $\text{Var}_{mod}$  the simulated variable and  $\text{Var}_{obs}$  the observed  
604 one, the mean bias expressed as

$$\text{Bias}_{xy} = \text{Var}_{mod_{xy}} - \text{Var}_{obs_{xy}} \quad (5)$$

605 measures the mean difference over the whole spatial domain and all time steps (12 climatological months).

606 The RMSE ( $rmS_{xyt}$ ) is the Root Mean Squared Error computed between the model and the  
607 reference over the twelve climatological months:

$$rmS_{xyt} = \sqrt{\frac{1}{T} \sum_{i,j,t} w_{i,j} (\text{Var}_{mod_{i,j,t}} - \text{Var}_{obs_{i,j,t}})^2} \quad (6)$$

608 The metric is sensitive to the value of the mean bias, and provides a measure of the spatio-temporal  
609 agreement between the model and the reference.

610 We present the global metrics only in the main text (see figure 3). We complete the analyses by  
611 computing the same metrics (bias and root mean square) at the seasonal time scale and for 3 latitudinal bands.  
612 We restrict the figure to surface air temperature and precipitation that reflects well the major differences. It  
613 shows that these measures capture differences between the IPSLCM5A-LR version of the IPSL model (Dufresne  
614 et al., 2013) and the new version developed for the TRHOLV transient simulation (see section 2). It also  
615 highlights the impact of running the model with the dynamical vegetation. However, as in Figure 3 the  
616 simulations with different MH conditions for the interactive vegetation, as well as the PI conditions obtained  
617 after 5900 years of transient simulation are difficult to distinguish. Differences become significant again when  
618 considering the last 50 years of the transient simulations that are affected by increase greenhouse gases.

## 619 6.2 A2 Biomization and sensitivity analysis.

620 Table A2 show the different ORCHIDEE PFT for the different MH and PI simulations, considering the  
621 regions that are affected, or regions that are not affected by land use in the pre-industrial simulation with  
622 vegetation prescribed to the 1860 observed values.

623

PFT	regions with landuse				regions without landuse							
	MH	MH	MH	PI	MH	MH	MH	PI	PI	PI	PI	Hist
	TRHOLV	Vnone	Vmap	1860	TRHOLV	Vnone	Vmap	TRHOLV	Vnone	Vmap	1860	TRHOLV
1 - Bare soil	9	9	8	12	21	22	22	24	23	28	26	23
2 - tropical broad-leaved evergreen	15	15	15	13	5	5	5	5	5	5	8	5
3 - tropical broad-leaved raingreen	8	8	8	11	3	3	3	3	3	3	2	3
4 - temperate needleleaf evergreen	8	8	8	5	1	1	1	1	1	1	2	1
5 - temperate broad-leaved evergreen	4	4	4	6	1	0	0	1	1	1	3	1
6 - temperate broad-leaved summergreen	9	8	8	8	2	2	2	2	2	2	2	2
7 - boreal needleleaf evergreen	9	9	9	2	13	13	11	8	10	9	8	11
8 - boreal broad-leaved summergreen	3	3	3	1	4	5	4	3	3	3	8	3
9 - boreal needleleaf summergreen	1	1	1	0	4	4	4	3	3	2	4	3
10 - C3 grass	17	17	16	23	37	36	36	41	41	39	32	38
11 - C4 grass	18	18	20	13	10	10	12	10	9	8	5	10
12 - C3 agriculture	0	0	0	4	0	0	0	0	0	0	0	0
13 - C4 agriculture	0	0	0	2	0	0	0	0	0	0	0	0

624 Table A2. Distribution of ORCHIDEE 13 PFTs (%) in different simulations and the PI 1860 map used  
625 as boundary conditions when vegetation is prescribed from pre industrial observations. If the PI 1860 fraction of  
626 land use in a grid box is larger than 0.01 then the grid box is considered as covered with land use. The  
627 percentage is computed for each region separately, each region having its own total area. The error bars are  
628 about 0.5, which is accounted for in the table by neglected decimals in the estimates.

629

630 To convert the ORCHIDEE model PFTs into mega biomes we use the algorithm proposed by Prentice  
631 et al. (2011) and used by Zhu et al. (2018). Figure A2a shows the different thresholds used in the algorithm. The  
632 black numbers correspond to the default values used to produce figure 14 in the main text. Since some of these  
633 thresholds are somehow artificially defined, we also tested the robustness of our comparison by running  
634 sensitivity tests. These tests considered successively different threshold in Growing Degree Days above 5°C  
635 (GDD5), canopy height and foliage projective cover as indicated in red on figure A2a.

636 The different thresholds induce only slight difference on the biome map for a given simulation. The  
637 largest sensitivity is obtained for the height. When 10 m is used instead of 6 m, a larger cover of savannah and  
638 dry woodland is estimated from the simulations in mid and high northern latitudes. In these latitudes also, a  
639 large sensitivity is found when the GDD5 limit is set to 500°C.d<sup>-1</sup> instead of 350°C.d<sup>-1</sup> between tundra and  
640 savannah and dry woodland or boreal forest.

641 The same analyses transformation into megabiomes was performed for the Vmap and Vnone  
642 simulations. Similar sensitivity is found to the different thresholds for these two simulations (Fig. A2 b). The  
643 synthesis of the goodness of fit between model and data is presented in figure A2 c. It shows that the two  
644 simulations provide as expected very similar results when compared to the MH BIOME6000 map. It is  
645 interesting to note that the different thresholds do not have a large impact on the model data comparison, when  
646 all data points are considered. The change in GDD5 limit produces tundra in better agreement with pollen data,  
647 and the canopy height better results with savannah and dry woodland. Note however that this result is in part due  
648 to the fact that there is little data in regions where the impact is the largest (Figure 6 in the main text).

649 The same procedure was also applied to the PI Vnone and PI-Vmap simulations. The overall  
650 correctness (percentage of reconstruction sites showing the same megabiome between model and data) is similar  
651 as the one obtained for MH (37% for MH and 35% for PI). These numbers are close to the percentages derived  
652 by Dallmeyer et al. (2019) using a climate-based biomization method (i.e. use ESM modeled climate states to  
653 force a biogeography model to simulate the biome distribution), which gives 33% and 39% with two IPSL model  
654 versions for pre-industrial

655 *Acknowledgments.* We would like to thanks our colleagues from the IPSL global climate model group  
656 for their help in setting up this intermediate version of the IPSL model. In particular the ORCHIDEE group  
657 provided good advices for the closure of the hydrological cycle in the land surface scheme (Philippe Peylin,  
658 Agnès Ducharne, Frédéric Cheruy and Joséfine Gattas) or the snow ablation (Sylvie Charbit and Christophe  
659 Dumas). The workflow for these long simulations benefits from the development of Anne Cozic and Arnaud  
660 Caubel. Discussions with Philippe Ciais and Yves Balkansky were also at the origin of the choice of the land  
661 surface model complexity and aerosols forcing strategy. We acknowledge PRACE for awarding us access to  
662 Curie at GENCI@CEA, France (THROL project) to start the simulations. The simulations were also performed  
663 using HPC resources from GENCI-TGCC thanks to a high end computing access grant and to our annual  
664 allocation time (gen2212). This work is supported by the JPI-Belmont PACMEDY project (N ° ANR-15-JCLI-  
665 0003-01).

666

667

Simulation	Comment	Initial state
<b>Reference MH) simulations with prescribed vegetation map</b>		
MH_PMIP3	Reference PMIP3-CMIP5 IPSL simulation (Kageyama et al., 2013a)	Previous MH long term simulation with the model used to test model configuration
MH_FPMIP4 (S_Sr04)	Reference version used here, with vegetation prescribed to the 1860 vegetation map as in PMIP3-CMIP5.	From year 250 of MH_L11AerEv below
<b>Reference PI simulations with prescribed vegetation map</b>		
PI_PMIP3	Reference PMIP3-CMIP5 IPSL simulation (Dufresne et al., 2013; Kageyama et al., 2013a)	
PI_FPMIP4	As L11AerEV but with pre industrial trace gases and Earth's orbital parameters	
<b>MH sensitivity experiments with prescribed vegetation map</b>		
MH_L11 (S_Sr01)	As PMIP3, but with new version of land surface model (hydrology and snow model)	From the last MH test of the new model configuration (new version of ORCHIDEE)
MH_L11Aer (S_Sr02)	As L11, but only dust and sea-salt considered in the aerosol forcing	Same as L11
MH_L11AerEv (S_Sr03)	As L11aer, but with factor to limit bare soil evaporation	From year 250 of L11Aer

668

669 Table 1. Tests done to set up the model IPSL version in which we included the dynamical vegetation.

670 For all these simulations the vegetation map is prescribed to the 1860 map used in PI-PMIP3. The different  
671 columns highlight the name of the test and the initial state to better isolate the different factors contributing to the  
672 adjustment curves in Figure 1. We include in parenthesis the tag of the simulation that corresponds to our  
673 internal nomenclature for memory.

674

675

Simulation	Comment	Initial state
<b>Reference Mid Holocene (MH) and PI simulations with dynamical vegetation</b>		
MH-Vnone (V-Sr09)	L11AerEv configuration but initial state with bare soil everywhere	Year 250 of L11AerEv for atmosphere ocean and sea ice
MH-Vnone_FPMIP4 (V-Sr12)*	Same simulation as MH-Vnone, but using the PMIP4 trace gases forcing	Year250 of MH-Vnone for all model components
PI-Vnone (V_Sr12) *	Preindustrial simulation corresponding to the MH simulations starting from bare soil	Year 500 of MH-Vnone-FPMIP4 for all model components
<b>Reference transient simulation of the last 6000 years with dynamical vegetation</b>		
TRHOLV	Transient mid Holocene to present day simulation with dynamical vegetation	Year 500 of MH-Vnone-FPMIP4 for all model components
<b>Sensitivity experiments to dynamical vegetation</b>		
MH-Vmap (V_Sr10)	As L11AerEv, but vegetation map and soil initial state from an off line ORCHIDEE vegetation force with L11 pre-industrial simulation	Year 250 or L11AerEv for atmosphere, ocean and sea-ice
MH-Vmap_FPMIP4 (V_Sr11)	Same simulation as MH-Vmap, but using the PMIP4 trace gases forcing	Year 200 of MH-Vmap, for all model components
PI-Vmap (V_Sr07)	Preindustrial simulation corresponding to the MH simulation starting from the off line ORCHIDEE vegetation force with L11 pre-industrial simulation	Year 250 of Vmap_FPMIP4, for all model components.

676

677 Table 2. Simulations run to initialize the dynamical vegetation starting from bare soil or from vegetation map and soil moisture resulting from an off line ORCHIDEE simulation with dynamical vegetation switch on and using the PI L11 simulated climate as boundary conditions. Simulations with an \* are considered as references for the model version and the transient simulations. We include in parentheses the tag of the simulation that corresponds to our internal nomenclature for memory.

682



683 7 Figure Caption

684 Figure 1: Illustration of the effect of the different adjustments made to produce mid-Holocene simulations with  
685 the modified version of the IPSLCM5A-MR version of the IPSL model in which the land surface model ORCHIDEE  
686 includes a different soil hydrology and snow models (see text for details). The three panels show the global  
687 average of a) net surface heat flux ( $\text{W.m}^{-2}$ ), b) evaporation ( $\text{kg.m}^{-2}$ ), and c) 2m air temperature ( $^{\circ}\text{C}$ ). The  
688 different color lines represent the results for the different simulations reported in Table 1.

690 Figure 2: Mid Holocene annual mean precipitation ( $\text{mm.d}^{-1}$ ) and 2m air temperature ( $^{\circ}\text{C}$ ) differences between  
691 a) and b) L11Aer and L11, c) and d) L11 and PMIP3, e) and f) PMIP3L11AerEv and L11Aer, and g) and h) FPMIP4  
692 and PMIP3. See Table 1 and text for the details about the different simulations.

694 Figure 3. a) Annual mean global model bias (bias\_xy) and b) spatio-temporal root mean square differences  
695 (rms\_xyt) computed on the annual cycle (twelve climatological months) over the globe for the different pre-  
696 industrial simulations considered in this manuscript (colors lines) and individual simulations of the CMIP5 multi-  
697 model ensemble (grey lines). The metrics for the different variables are presented as parallel coordinates, each  
698 of them having their own vertical axis with corresponding values. In these plots, ta stands for temperature ( $^{\circ}\text{C}$ )  
699 with s for surface, 850 and 200 for 850 and 300 hPa respectively, prw for total water content ( $\text{g.kg}^{-1}$ ), pr for  
700 precipitation ( $\text{mm.d}^{-1}$ ), rlut for outgoing long wave radiation ( $\text{W.m}^{-2}$ ), rltcre and rltcre for the cloud radiative  
701 effect at the top of the atmosphere in the short wave and long wave radiation respectively ( $\text{W.m}^{-2}$ ). See annex  
702 A1 for details on the metrics.

704 Figure 4. Long term adjustment of vegetation for a), b), and c) mid Holocene (MH) and c), d) and e)  
705 preindustrial (PI) climate, when starting from bare soil (Vnone) or from a vegetation map (Vmap). The 13  
706 ORCHIDEE PFTs have been gathered as bare soil, grass, tree and land-use. When the dynamical vegetation is  
707 active only natural vegetation is considered. Land-use is thus only present in one simulation, corresponding to a  
708 pre-industrial map used as reference in the IPSL model (Dufresne et al. 2013). The corresponding vegetation is  
709 referred to as PI\_prescribed. The x axis is in months, starting from 0, which allows to plot all the simulation that  
710 have their own internal calendar on the same axis.

712 Figure 5: Evolution of trace gases:  $\text{CO}_2$  (ppm),  $\text{CH}_4$  (ppb) and  $\text{N}_2\text{O}$  (ppb), and seasonal amplitude (maximum  
713 annual – minimum annual monthly values) of the incoming solar radiation at the top of the atmosphere ( $\text{W.m}^{-2}$ )  
714 averaged over the northern (black line) and the southern (red line) hemispheres. These forcing factors  
715 correspond to the PMIP4 experimental design discussed by Otto-Bliesner et al. (2017).

717 Figure 6. Long term evolution of incoming solar radiation at the top of the atmosphere (TOA) ( $\text{Wm}^{-2}$ , top panel)  
718 and associated response of temperature ( $^{\circ}\text{C}$ ) and precipitation ( $\text{mm.y}^{-1}$ ) expressed as a difference with the  
719 6000 year PB initial state and smoothed by a 100 year running mean) for a) NH Summer, b) NH winter, c) SH  
720 summer, and d) SH winter. Temperatures are plotted in red and precipitation in blue for summer, and they are  
721 respectively plotted in orange and green for winter. NH Summer and SH Winter correspond to June to  
722 September averages whereas NH winter and SH summer correspond to December to March averages. All  
723 curves, except insolation, have been smoothed by a 100 year running mean.

725 Figure 7: Fraction of the evolution of the seasonal amplitude of temperature (red) and precipitation (blue)  
726 represented by the projection of these climate variables on the evolution of the seasonal amplitude of  
727 insolation as a function of latitude. The solid line stands for the raw signal and the dotted line for the signal  
728 after a 100 year smoothing.

730 Figure 8: a) total change in snow cover ( $\text{kg m}^{-2}$ ) and sea ice fraction (%) integrated over the last 6000 years, and  
731 evolution from the Mid Holocene of annual mean maximum summer and minimum winter values for b) sea ice  
732 averages over the northern hemisphere, c) snow (solid lines) and 2-m air temperature (dotted lines) average  
733 for all regions north of  $60^{\circ}\text{N}$ , and d) snow and 2m air temperature over Eurasia. In b), c), and d) black, dark blue  
734 and light blue stand respectively for the annual mean, maximum and minimum annual monthly values for sea-  
735 ice or snow cover, and black, green and red for annual mean, annual minimum and annual maximum air  
736 temperature.

738 Figure 9: Long term evolution of the simulated a) bare soil, b) grass and c) tree covers, expressed as the  
739 percentage (%) of Global, NH or SH continental areas, and d) GPP (PgC/y) over the same regions. Annual mean  
740 values are smoothed by a 100 year running mean.

741  
742 Figure 10: Vegetation map comparing a), d), g) the Mid Holocene (first 50 years) and the pre-industrial (50 year  
743 around 1850 AC (last 150 to 100 years) periods of the transient simulation, b), d), h) the differences between  
744 the historical period (last 50 years) and the pre-industrial period of the transient simulation and c), f), i) the  
745 difference between pre-industrial climate for the transient simulation and the PI-Vnone simulations. For  
746 simplicity we only consider bare soil (top), grass (middle) and tree (bottom).

747  
748 Figure 11: Long term evolution of Bare soil, Grass and Tree, expressed as the % of land cover North of 60°N,  
749 over Eurasia and over West Africa. The different values are plotted as differences with the first 100 year  
750 averages. A 100 year running mean is applied to the curves before plotting.

751  
752 Figure 12. Evolution of a) the location of the West African monsoon annual mean (black) and maximum (red)  
753 rain belt in degrees of latitude and b) annual mean (black), minimum (green) and maximum (red) monthly  
754 precipitation ( $\text{mm}\cdot\text{d}^{-1}$ ) averages over the Sahel region. The first 100 years have been removed and a 100  
755 running mean applied before plotting.

756  
757 Figure 13: Evolution of the different tree PFTs in Eurasia, expressed as the percentage change compared to  
758 their 6000 year BP initial state. Each color line stands for a different PFT. Values have been smoothed by a 100  
759 year running mean.

760  
761 Figure 14: a) Simulated mega-biome distribution by MH-Vnone, converted from the modelled PFT properties  
762 using the default algorithm described in Figure A1. b) and c) Reconstructions in BIOME 6000 DB version 1 for  
763 the MH and PI periods (Harrison, 2017). d) Number of pixels where reconstruction is available and the model  
764 matches (or does not match) the data. Note that multiple reconstruction sites may be located in the same  
765 model grid cell, in which case we did not group them so that each site was counted once. Numbers in  
766 parenthesis on the x axis in d) represent the number of sites for each biome type. Same as in c) but for the  
767 number of matches between e) the BIOME6000 MH (6k) and PI (0k) reconstructions at pollen sites and f) the  
768 simulated mega-biomes for MH and PI at each model grid cell.

769  
770 Figure 15: Impact of the dynamical vegetation and initialization of vegetation on the simulated climate.  
771 Differences for annual mean a) c) e) precipitation ( $\text{mm}\cdot\text{d}^{-1}$ ) and b) d) f) 2m air temperature ( $^{\circ}\text{C}$ ) between a) and  
772 b) the MH in the TRHOLV simulation and the MH simulation without dynamical vegetation (MH FPMIP4), d)  
773 and d) the mid Holocene and the pre-industrial simulations in the TTHOLV simulation, and e) and f) the two  
774 pre-industrial simulations initialized from bare soil (PI-Vnone) or a vegetation map for vegetation (PI-Vmap).  
775 See table 2 and text for details on the simulations.

776  
777  
778 Figure 16: Difference between Vegetation maps obtained with the two different initial states for a) c) e) mid  
779 Holocene simulations, b) d) f) pre-industrial simulations. Vmap stands for MH and PI simulations where the  
780 mid-Holocene vegetation has been initialized from a vegetation map and Vnone for MH and PI simulations  
781 where the mid-Holocene has been initialized from bare soil. For simplicity we only consider fractions of a) b)  
782 bare soil, c) d) grass and e) f) trees.

783  
784  
785 Figure A1: Parallel coordinate representation of metrics highlighting model mean bias (left column) and spatial  
786 root mean square differences (right column) against observations for the four climatological seasons  
787 (December to February, djf; Mars to May, mam; June to August, jja; September to November, son) for surface  
788 air temperature ( $\text{tas}$ ,  $^{\circ}\text{C}$ ) and precipitation ( $\text{mmd}^{-1}$ ) and Northern Hemisphere extra tropics (NHEX, 20°N-90°N),  
789 Tropics (20°S-20°N), and Southern Hemisphere extra tropics (SHEX 90°S-20°S). Each color line stands for a  
790 simulations discussed in this manuscript. The results of the different CMIP5 simulations (grey lines) are  
791 included for comparison.

792  
793 Figure A2 : (a) Algorithm to convert the modelled PFT properties into the eight megabiomes provided by  
794 BIOME 6000 DB version 1. The default thresholds (in black) are the same as Zhu et al. (2018), while different

795 values (in red) are tested: GDD<sub>5</sub> (annual growing degree days above 5 °C) of 500 K days (Joos et al., 2004), FPC  
796 (foliage projective cover) of 0.3 and 0.6 (Prentice et al., 2011) Height (average height of all existing tree PFTs) of  
797 10 m (Prentice et al., 2011). (b) Simulated megabiome distribution by MH\_Vnone and MH\_Vmap, using  
798 different conversion methods in (a). (c) The number of pixels where modelled megabiome matches data for  
799 each biome type, divided by the total number of available sites for that biome type.

800

801

802

803

804

806

807 Abis, B. and Brovkin, V.: Environmental conditions for alternative tree-cover states in high latitudes,  
808 *Biogeosciences*, 14, 511-527, 2017.

809 Albani, S., Mahowald, N. M., Winckler, G., Anderson, R. F., Bradtmiller, L. I., Delmonte, B., François,  
810 R., Goman, M., Heavens, N. G., Hesse, P. P., Hovan, S. A., Kang, S. G., Kohfeld, K. E., Lu, H., Maggi, V.,  
811 Mason, J. A., Mayewski, P. A., McGee, D., Miao, X., Otto-Bliesner, B. L., Perry, A. T., Pourmand, A.,  
812 Roberts, H. M., Rosenbloom, N., Stevens, T., and Sun, J.: Twelve thousand years of dust: the  
813 Holocene global dust cycle constrained by natural archives, *Clim. Past*, 11, 869-903, 2015.

814 Alexandrov, D. V., Bashkirtseva, I. A., and Ryashko, L. B.: Noise-induced transitions and shifts in a  
815 climate–vegetation feedback model, *Royal Society Open Science*, 5, 2018.

816 Aumont, O. and Bopp, L.: Globalizing results from ocean in situ iron fertilization studies, *Global  
817 Biogeochemical Cycles*, 20, -, 2006.

818 Bartlein, P. J., Harrison, S. P., Brewer, S., Connor, S., Davis, B. A. S., Gajewski, K., Guiot, J., Harrison-  
819 Prentice, T. I., Henderson, A., Peyron, O., Prentice, I. C., Scholze, M., Seppa, H., Shuman, B., Sugita,  
820 S., Thompson, R. S., Viau, A. E., Williams, J., and Wu, H.: Pollen-based continental climate  
821 reconstructions at 6 and 21 ka: a global synthesis, *Climate Dynamics*, 37, 775-802, 2011.

822 Bathiany, S., Claussen, M., and Fraedrich, K.: Implications of climate variability for the detection of  
823 multiple equilibria and for rapid transitions in the atmosphere-vegetation system, *Climate  
824 Dynamics*, 38, 1775-1790, 2012.

825 Berger, A.: Long-term variations of caloric solar radiation resulting from the Earth's orbital elements,  
826 *Quaternary Research*, 9, 139-167, 1978.

827 Bigelow, N. H., Brubaker, L. B., Edwards, M. E., Harrison, S. P., Prentice, I. C., Anderson, P. M.,  
828 Andreev, A. A., Bartlein, P. J., Christensen, T. R., Cramer, W., Kaplan, J. O., Lozhkin, A. V.,  
829 Matveyeva, N. V., Murray, D. F., McGuire, A. D., Razzhivin, V. Y., Ritchie, J. C., Smith, B., Walker, D.  
830 A., Gajewski, K., Wolf, V., Holmqvist, B. H., Igarashi, Y., Kremenetskii, K., Paus, A., Pisaric, M. F. J.,  
831 and Volkova, V. S.: Climate change and Arctic ecosystems: 1. Vegetation changes north of 55  
832 degrees N between the last glacial maximum, mid-Holocene, and present, *Journal of Geophysical  
833 Research-Atmospheres*, 108, 2003.

834 Boisier, J., Noblet - Ducoudré, N. d., Pitman, A., Cruz, F., Delire, C., den Hurk, B., Molen, M., Müller,  
835 C., and Voltaire, A.: Attributing the impacts of land - cover changes in temperate regions on  
836 surface temperature and heat fluxes to specific causes: Results from the first LUCID set of  
837 simulations, *Journal of Geophysical Research: Atmospheres*, 117, 2012.

838 Bonfils, C., de Noblet-Ducoure, N., Braconnot, P., and Joussaume, S.: Hot desert albedo and climate  
839 change: Mid-Holocene monsoon in North Africa, *Journal of Climate*, 14, 3724-3737, 2001.

840 Braconnot, P., Harrison, S. P., Kageyama, M., Bartlein, P. J., Masson-Delmotte, V., Abe-Ouchi, A.,  
841 Otto-Bliesner, B., and Zhao, Y.: Evaluation of climate models using palaeoclimatic data, *Nature  
842 Climate Change*, 2, 417-424, 2012.

843 Braconnot, P., Joussaume, S., Marti, O., and de Noblet, N.: Synergistic feedbacks from ocean and  
844 vegetation on the African monsoon response to mid-Holocene insolation, *Geophys .Res. Lett.*, 26,  
845 2481-2484, 1999.

846 Braconnot, P. and Kageyama, M.: Shortwave forcing and feedbacks in Last Glacial Maximum and Mid-  
847 Holocene PMIP3 simulations, *Phil. Trans. R. Soc. A*, 373, 20140424, 2015.

848 Braconnot, P., Marti, O., and Joussaume, S.: Adjustment and feedbacks in a global coupled ocean-  
849 atmosphere model, *Climate Dynamics*, 13, 507-519, 1997.

850 Braconnot, P., Otto-Bliesner, B., Harrison, S., Joussaume, S., Peterchmitt, J. Y., Abe-Ouchi, A., Crucifix,  
851 M., Driesschaert, E., Fichet, T., Hewitt, C. D., Kageyama, M., Kitoh, A., Laine, A., Loutre, M. F.,  
852 Marti, O., Merkel, U., Ramstein, G., Valdes, P., Weber, S. L., Yu, Y., and Zhao, Y.: Results of PMIP2  
853 coupled simulations of the Mid-Holocene and Last Glacial Maximum - Part 1: experiments and  
854 large-scale features, *Climate of the Past*, 3, 261-277, 2007a.

855 Braconnot, P., Otto-Bliesner, B., Harrison, S., Joussaume, S., Peterchmitt, J. Y., Abe-Ouchi, A., Crucifix,  
856 M., Driesschaert, E., Fichefet, T., Hewitt, C. D., Kageyama, M., Kitoh, A., Loutre, M. F., Marti, O.,  
857 Merkel, U., Ramstein, G., Valdes, P., Weber, L., Yu, Y., and Zhao, Y.: Results of PMIP2 coupled  
858 simulations of the Mid-Holocene and Last Glacial Maximum - Part 2: feedbacks with emphasis on  
859 the location of the ITCZ and mid- and high latitudes heat budget, *Climate of the Past*, 3, 279-296,  
860 2007b.

861 Brovkin, V., Bendtsen, J., Claussen, M., Ganopolski, A., Kubatzki, C., Petoukhov, V., and Andreev, A.:  
862 Carbon cycle, vegetation, and climate dynamics in the Holocene: Experiments with the CLIMBER-2  
863 model, *Global Biogeochemical Cycles*, 16, 2002.

864 Campbell, J. E., Berry, J. A., Seibt, U., Smith, S. J., Montzka, S. A., Launois, T., Belviso, S., Bopp, L., and  
865 Laine, M.: Large historical growth in global terrestrial gross primary production, *Nature*, 544, 84,  
866 2017.

867 Claussen, M.: Late Quaternary vegetation-climate feedbacks, *Climate of the Past*, 5, 203-216, 2009.

868 Claussen, M. and Gayler, V.: The greening of the Sahara during the mid-Holocene: results of an  
869 interactive atmosphere-biome model, *Global Ecology and Biogeography Letters*, 6, 369-377, 1997.

870 COHMAP-Members: Climatic changes of the last 18,000 years: observations and model simulations,  
871 *Science*, 241, 1043-1052, 1988.

872 Crucifix, M., Loutre, M. F., Tulkens, P., Fichefet, T., and Berger, A.: Climate evolution during the  
873 Holocene: a study with an Earth system model of intermediate complexity, *Climate Dynamics*, 19,  
874 43-60, 2002.

875 d'Orgeval, T., Polcher, J., and de Rosnay, P.: Sensitivity of the West African hydrological cycle in  
876 ORCHIDEE to infiltration processes, *Hydrol. Earth Syst. Sci.*, 12, 1387-1401, 2008.

877 Dallmeyer, A., Claussen, M., and Brovkin, V.: Harmonising plant functional type distributions for  
878 evaluating Earth system models, *Clim. Past*, 15, 335-366, 2019.

879 Dallmeyer, A., Claussen, M., and Otto, J.: Contribution of oceanic and vegetation feedbacks to  
880 Holocene climate change in monsoonal Asia, *Clim. Past*, 6, 195-218, 2010.

881 Davis, B. A. S., Brewer, S., Stevenson, A. C., and Guiot, J.: The temperature of Europe during the  
882 Holocene reconstructed from pollen data, *Quaternary Science Reviews*, 22, 1701-1716, 2003.

883 de Noblet-Ducoudre, N., Claussen, R., and Prentice, C.: Mid-Holocene greening of the Sahara: first  
884 results of the GAIM 6000 year BP Experiment with two asynchronously coupled atmosphere/biome  
885 models, *Climate Dynamics*, 16, 643-659, 2000.

886 de Noblet, N., Prentice, I. C., Joussaume, S., Texier, D., Botta, A., and Haxeltine, A.: Possible role of  
887 atmosphere-biosphere interactions in triggering the last glaciation, *Geophys. Res. Letters*, 23, 3191-  
888 3194, 1996.

889 de Rosnay, P., Polcher, J., Bruen, M., and Laval, K.: Impact of a physically based soil water flow and  
890 soil-plant interaction representation for modeling large-scale land surface processes, *Journal of*  
891 *Geophysical Research-Atmospheres*, 107, 2002.

892 deMenocal, P., Ortiz, J., Guilderson, T., Adkins, J., Sarnthein, M., Baker, L., and Yarusinsky, M.: Abrupt  
893 onset and termination of the African Humid Period: rapid climate responses to gradual insolation  
894 forcing, *Quaternary Science Reviews*, 19, 347-361, 2000.

895 Ducoudré, N., Laval, K., and Perrier, A.: SECHIBA, a new set of parameterizations of the hydrologic  
896 exchanges at the land/atmosphere interface within the LMD atmospheric general circulation  
897 model, *Journal of Climate*, 6, 1993.

898 Dufresne, J. L., Foujols, M. A., Denvil, S., Caubel, A., Marti, O., Aumont, O., Balkanski, Y., Bekki, S.,  
899 Bellenger, H., Benschila, R., Bony, S., Bopp, L., Braconnot, P., Brockmann, P., Cadule, P., Cheruy, F.,  
900 Codron, F., Cozic, A., Cugnet, D., de Noblet, N., Duvel, J. P., Ethe, C., Fairhead, L., Fichefet, T.,  
901 Flavoni, S., Friedlingstein, P., Grandpeix, J. Y., Guez, L., Guilyardi, E., Hauglustaine, D., Hourdin, F.,  
902 Idelkadi, A., Ghattas, J., Joussaume, S., Kageyama, M., Krinner, G., Labetoulle, S., Lahellec, A.,  
903 Lefebvre, M. P., Lefevre, F., Levy, C., Li, Z. X., Lloyd, J., Lott, F., Madec, G., Mancip, M., Marchand,  
904 M., Masson, S., Meurdesoif, Y., Mignot, J., Musat, I., Parouty, S., Polcher, J., Rio, C., Schulz, M.,  
905 Swingedouw, D., Szopa, S., Talandier, C., Terray, P., Viovy, N., and Vuichard, N.: Climate change

906 projections using the IPSL-CM5 Earth System Model: from CMIP3 to CMIP5, *Climate Dynamics*, 40,  
907 2123-2165, 2013.

908 ▲ Egerer, S., Claussen, M., Reick, C., and Stanelle, T.: Could gradual changes in Holocene Saharan  
909 landscape have caused the observed abrupt shift in North Atlantic dust deposition?, *Earth and*  
910 *Planetary Science Letters*, 473, 104-112, 2017.

911 Fichefet, T. and Maqueda, M. A. M.: Modelling the influence of snow accumulation and snow-ice  
912 formation on the seasonal cycle of the Antarctic sea-ice cover, *Climate Dynamics*, 15, 251-268,  
913 1999.

914 Gleckler, P., Doutriaux, C., Durack, P., Taylor, K., Zhang, Y., Williams, D., Mason, E., and Servonnat, J.:  
915 A More Powerful Reality Test for Climate Models, *EOS, Transactions of the American Geophysical*  
916 *Union*, 97, 2016.

917 Guimberteau, M., Zhu, D., Maignan, F., Huang, Y., Yue, C., Dantec-Nédélec, S., Ottlé, C., Jornet-Puig,  
918 A., Bastos, A., Laurent, P., Goll, D., Bowring, S., Chang, J., Guenet, B., Tifafi, M., Peng, S., Krinner, G.,  
919 Ducharne, A., Wang, F., Wang, T., Wang, X., Wang, Y., Yin, Z., Lauerwald, R., Joetzjer, E., Qiu, C.,  
920 Kim, H., and Ciais, P.: ORCHIDEE-MICT (v8.4.1), a land surface model for the high latitudes: model  
921 description and validation, *Geosci. Model Dev.*, 11, 121-163, 2018.

922 Harrison, S.: BIOME 6000 DB classified plotfile version 1, University of Reading. Dataset. , doi:  
923 <http://dx.doi.org/10.17864/1947.99>, 2017. 2017.

924 Harrison, S. P., Bartlein, P. J., Brewer, S., Prentice, I. C., Boyd, M., Hessler, I., Holmgren, K., Izumi, K.,  
925 and Willis, K.: Climate model benchmarking with glacial and mid-Holocene climates, *Climate*  
926 *Dynamics*, 43, 671-688, 2014.

927 Harrison, S. P., Jolly, D., Laarif, F., Abe-Ouchi, A., Dong, B., Herterich, K., Hewitt, C., Jousaume, S.,  
928 Kutzbach, J. E., Mitchell, J., de Noblet, N., and Valdes, P.: Intercomparison of Simulated Global  
929 Vegetation Distributions in Response to 6 kyr BP Orbital Forcing, *Journal of Climate*, 11, 2721-2742,  
930 1998.

931 Held, I. M. and Soden, B. J.: Robust Responses of the Hydrological Cycle to Global Warming, *Journal*  
932 *of Climate*, 19, 5686-5699, 2006.

933 Hély, C. and Lézine, A.-M.: Holocene changes in African vegetation: tradeoff between climate and  
934 water availability, *Climate of the Past*, 10, 681-686, 2014.

935 Hopcroft, P. O., Valdes, P. J., Harper, A. B., and Beerling, D. J.: Multi vegetation model evaluation of  
936 the Green Sahara climate regime, *Geophysical Research Letters*, 44, 6804-6813, 2017.

937 Hourdin, F., Foujols, M. A., Codron, F., Guemas, V., Dufresne, J. L., Bony, S., Denvil, S., Guez, L., Lott,  
938 F., Ghattas, J., Braconnot, P., Marti, O., Meurdesoif, Y., and Bopp, L.: Impact of the LMDZ  
939 atmospheric grid configuration on the climate and sensitivity of the IPSL-CM5A coupled model,  
940 *Climate Dynamics*, 40, 2167-2192, 2013.

941 Jansen, E., Overpeck, J., Briffa, K. R., Duplessy, J. C., Joos, F., Masson-Delmotte, V., Olago, D., Otto-  
942 Bliesner, B., Peltier, W. R., Rahmstorf, S., Ramesh, R., Raynaud, D., Rind, D., Solomina, O., Villalba,  
943 R., and Zhang, D.: Paleoclimate. In: *Climate Change 2007: The Physical Science Basis. Contribution of*  
944 *Working Group I to the Fourth Assessment Report of the Intergovernmental Panel on Climate*  
945 *Change*, Solomon, S., Qin, D. H., Manning, M., Chen, Z., Marsuis, M., Averyt, K. B., Tignor, M., and  
946 Miller, H. L. (Eds.), Cambridge University Press, Cambridge, United Kingdom and New York, NY, USA,  
947 2007.

948 Jolly, D., Prentice, I. C., Bonnefille, R., Ballouche, A., Bengo, M., Brenac, P., Buchet, G., Burney, D.,  
949 Cazet, J.-P., Cheddadi, R., Edohr, T., Elenga, H., Elmoutaki, S., Guiot, J., Laarif, F., Lamb, H., Lezine,  
950 A.-M., Maley, J., Mbenza, M., Peyron, O., Reille, M., Reynaud-Ferrera, I., Riollet, G., Ritchie, J. C.,  
951 Roche, E., Scott, L., Ssemmanda, I., Straka, H., Umer, M., Van Campo, E., Vilimumbala, S., Vincens,  
952 A., and Waller, M.: Biome reconstruction from pollen and plant macrofossil data for Africa and the  
953 Arabian peninsula at 0 and 6 ka., *Journal of Biogeography*, 25, 1007-1028, 1998.

954 Jomelli, V., Khodri, M., Favier, V., Brunstein, D., Ledru, M. P., Wagnon, P., Blard, P. H., Sicart, J. E.,  
955 Braucher, R., Grancher, D., Bourles, D. L., Braconnot, P., and Vuille, M.: Irregular tropical glacier  
956 retreat over the Holocene epoch driven by progressive warming, *Nature*, 474, 196-199, 2011.

- 957 Joos, F., Gerber, S., Prentice, I., Otto-Bliesner, B., and Valdes, P.: Transient simulations of Holocene  
958 atmospheric carbon dioxide and terrestrial carbon since the Last Glacial Maximum, *GLOBAL*  
959 *BIOGEOCHEMICAL CYCLES*, 18, -, 2004.
- 960 ▲ Joos, F. and Spahni, R.: Rates of change in natural and anthropogenic radiative forcing over the past  
961 20,000 years, *Proceedings of the National Academy of Sciences*, 105, 1425-1430, 2008.
- 962 Jousaume, S. and Braconnot, P.: Sensitivity of paleoclimate simulation results to season definitions,  
963 *J. Geophys. Res.*, 102, 1943-1956, 1997.
- 964 Jousaume, S., Taylor, K. E., Braconnot, P., Mitchell, J. F. B., Kutzbach, J. E., Harrison, S. P., Prentice, I.  
965 C., Broccoli, A. J., Abe-Ouchi, A., Bartlein, P. J., Bonfils, C., Dong, B., Guiot, J., Herterich, K., Hewitt, C.  
966 D., Jolly, D., Kim, J. W., Kislov, A., Kitoh, A., Loutre, M. F., Masson, V., McAvaney, B., McFarlane, N.,  
967 de Noblet, N., Peltier, W. R., Peterschmitt, J. Y., Pollard, D., Rind, D., Royer, J. F., Schlesinger, M. E.,  
968 Syktus, J., Thompson, S., Valdes, P., Vettoretti, G., Webb, R. S., and Wypytta, U.: Monsoon changes  
969 for 6000 years ago: Results of 18 simulations from the Paleoclimate Modeling Intercomparison  
970 Project (PMIP), *Geophysical Research Letters*, 26, 859-862, 1999.
- 971 Kageyama, M., Braconnot, P., Bopp, L., Caubel, A., Foujols, M. A., Guilyardi, E., Khodri, M., Lloyd, J.,  
972 Lombard, F., Mariotti, V., Marti, O., Roy, T., and Woillez, M. N.: Mid-Holocene and Last Glacial  
973 Maximum climate simulations with the IPSL model-part I: comparing IPSL\_CM5A to IPSL\_CM4,  
974 *Climate Dynamics*, 40, 2447-2468, 2013a.
- 975 Kageyama, M., Braconnot, P., Bopp, L., Mariotti, V., Roy, T., Woillez, M. N., Caubel, A., Foujols, M. A.,  
976 Guilyardi, E., Khodri, M., Lloyd, J., Lombard, F., and Marti, O.: Mid-Holocene and last glacial  
977 maximum climate simulations with the IPSL model: part II: model-data comparisons, *Climate*  
978 *Dynamics*, 40, 2469-2495, 2013b.
- 979 Kageyama, M., Braconnot, P., Harrison, S. P., Haywood, A. M., Jungclaus, J. H., Otto-Bliesner, B. L.,  
980 Peterschmitt, J. Y., Abe-Ouchi, A., Albani, S., Bartlein, P. J., Brierley, C., Crucifix, M., Dolan, A.,  
981 Fernandez-Donado, L., Fischer, H., Hopcroft, P. O., Ivanovic, R. F., Lambert, F., Lunt, D. J.,  
982 Mahowald, N. M., Peltier, W. R., Phipps, S. J., Roche, D. M., Schmidt, G. A., Tarasov, L., Valdes, P. J.,  
983 Zhang, Q., and Zhou, T.: The PMIP4 contribution to CMIP6 – Part 1: Overview and over-arching  
984 analysis plan, *Geosci. Model Dev.*, 11, 1033-1057, 2018.
- 985 Krinner, G., Viovy, N., de Noblet-Ducoudre, N., Ogee, J., Polcher, J., Friedlingstein, P., Ciais, P., Sitch,  
986 S., and Prentice, I. C.: A dynamic global vegetation model for studies of the coupled atmosphere-  
987 biosphere system, *Global Biogeochemical Cycles*, 19, -, 2005.
- 988 Kutzbach, J. E., Bartlein, P. J., Foley, J. A., Harrison, S. P., Hostetler, S. W., Liu, Z., Prentice, I. C., and  
989 Webb, T.: Potential role of vegetation feedback in the climate sensitivity of high-latitude regions: A  
990 case study at 6000 years BP, *Global Biogeochemical Cycles*, 10, 727-736, 1996.
- 991 Lenton, T. M., Held, H., Kriegler, E., Hall, J. W., Lucht, W., Rahmstorf, S., and Schellnhuber, H. J.:  
992 Tipping elements in the Earth's climate system, *Proceedings of the National Academy of Sciences*,  
993 105, 1786-1793, 2008.
- 994 Levis, S., Bonan, G. B., and Bonfils, C.: Soil feedback drives the mid-Holocene North African monsoon  
995 northward in fully coupled CCSM2 simulations with a dynamic vegetation model, *Climate Dynamics*,  
996 23, 791-802, 2004.
- 997 Lezine, A. M., Hely, C., Grenier, C., Braconnot, P., and Krinner, G.: Sahara and Sahel vulnerability to  
998 climate changes, lessons from Holocene hydrological data, *Quaternary Science Reviews*, 30, 3001-  
999 3012, 2011.
- 1000 Lezine, A. M., Ivory, S. J., Braconnot, P., and Marti, O.: Timing of the southward retreat of the ITCZ at  
1001 the end of the Holocene Humid Period in Southern Arabia: Data-model comparison, *Quaternary*  
1002 *Science Reviews*, 164, 68-76, 2017.
- 1003 Liu, Z., Wang, Y., Gallimore, R., Gasse, F., Johnson, T., deMenocal, P., Adkins, J., Notaro, M., Prentice,  
1004 I. C., Kutzbach, J., Jacob, R., Behling, P., Wang, L., and Ong, E.: Simulating the transient evolution  
1005 and abrupt change of Northern Africa atmosphere-ocean-terrestrial ecosystem in the Holocene,  
1006 *Quaternary Science Reviews*, 26, 1818-1837, 2007.
- 1007 Madec, G.: NEMO ocean engine, 2008.

- 1008 Marti, O., Braconnot, P., Dufresne, J. L., Bellier, J., Benshila, R., Bony, S., Brockmann, P., Cadule, P.,  
1009 Caubel, A., Codron, F., de Noblet, N., Denvil, S., Fairhead, L., Fichet, T., Foujols, M. A.,  
1010 Friedlingstein, P., Goosse, H., Grandpeix, J. Y., Guilyardi, E., Hourdin, F., Idelkadi, A., Kageyama, M.,  
1011 Krinner, G., Levy, C., Madec, G., Mignot, J., Musat, I., Swingedouw, D., and Talandier, C.: Key  
1012 features of the IPSL ocean atmosphere model and its sensitivity to atmospheric resolution, *Climate*  
1013 *Dynamics*, 34, 1-26, 2010.
- 1014 Mauri, A., Davis, B., Collins, P., and Kaplan, J.: The climate of Europe during the Holocene: a gridded  
1015 pollen-based reconstruction and its multi-proxy evaluation, *Quaternary Science Reviews*, 112, 109-  
1016 127, 2015.
- 1017 Otto-Bliesner, B., Braconnot, P., Harrison, S., Lunt, D., Abe-Ouchi, A., Albani, S., Bartlein, P., Capron,  
1018 E., Carlson, A., Dutton, A., Fischer, H., Goelzer, H., Govin, A., Haywood, A., Joos, F., LeGrande, A.,  
1019 Lipscomb, W., Lohmann, G., Mahowald, N., Nehrbass-Ahles, C., Pausata, F., Peterschmitt, J.-Y.,  
1020 Phipps, S., Renssen, H., and Zhang, Q.: The PMIP4 contribution to CMIP6 – Part 2: Two interglacials,  
1021 scientific objective and experimental design for Holocene and Last Interglacial simulations,  
1022 *Geoscientific Model Development*, 10, 3979-4003, 2017.
- 1023 Otto, J., Raddatz, T., and Claussen, M.: Strength of forest-albedo feedback in mid-Holocene climate  
1024 simulations, *Clim. Past*, 7, 1027-1039, 2011.
- 1025 Otto, J., Raddatz, T., Claussen, M., Brovkin, V., and Gayler, V.: Separation of atmosphere-ocean-  
1026 vegetation feedbacks and synergies for mid-Holocene climate, *Geophysical Research Letters*, 36,  
1027 2009.
- 1028 Pausata, F. S., Messori, G., and Zhang, Q.: Impacts of dust reduction on the northward expansion of  
1029 the African monsoon during the Green Sahara period, *Earth and Planetary Science Letters*, 434,  
1030 298-307, 2016.
- 1031 Prentice, I. C., Harrison, S. P., and Bartlein, P. J.: Global vegetation and terrestrial carbon cycle  
1032 changes after the last ice age, *New Phytologist*, 189, 988-998, 2011.
- 1033 Prentice, I. C. and Webb, T.: BIOME 6000: reconstructing global mid-Holocene vegetation patterns  
1034 from palaeoecological records, *Journal of Biogeography*, 25, 997-1005, 1998.
- 1035 Renssen, H., Seppä, H., Crosta, X., Goosse, H., and Roche, D. M.: Global characterization of the  
1036 Holocene Thermal Maximum, *Quaternary Science Reviews*, 48, 7-19, 2012.
- 1037 Saint-Lu, M., Braconnot, P., Leloup, J., and Marti, O.: The role of El Niño in the global energy  
1038 redistribution: a case study in the mid-Holocene, *Climate Dynamics*, 2016. 1-18, 2016.
- 1039 Scheffer, M., Hirota, M., Holmgren, M., Van Nes, E. H., and Chapin, F. S.: Thresholds for boreal biome  
1040 transitions, *Proceedings of the National Academy of Sciences*, 109, 21384-21389, 2012.
- 1041 Singarayer, J. S. and Valdes, P. J.: High-latitude climate sensitivity to ice-sheet forcing over the last  
1042 120 kyr, *Quaternary Science Reviews*, 29, 43-55, 2010.
- 1043 Texier, D., de Noblet, N., Harrison, S. P., Haxeltine, A., Jolly, D., Joussaume, S., Laarif, F., Prentice, I. C.,  
1044 and Tarasov, P.: Quantifying the role of biosphere-atmosphere feedbacks in climate change:  
1045 coupled model simulations for 6000 years BP and comparison with palaeodata for northern Eurasia  
1046 and northern Africa, *Climate Dynamics*, 13, 865-882, 1997.
- 1047 Torres, O., Braconnot, P., Marti, O., and Gential, L.: Impact of air-sea drag coefficient for latent heat  
1048 flux on large scale climate in coupled and atmosphere stand-alone simulations, *Climate Dynamics*,  
1049 2018. 1-20, 2018.
- 1050 Valcke, S.: OASIS3 user's guide (prism-2-5). CERFACS, Toulouse, France, 2006.
- 1051 Vial, J., Dufresne, J. L., and Bony, S.: On the interpretation of inter-model spread in CMIP5 climate  
1052 sensitivity estimates, *Climate Dynamics*, 41, 3339-3362, 2013.
- 1053 Wang, T., Ottlé, C., Boone, A., Ciais, P., Brun, E., Morin, S., Krinner, G., Piao, S., and Peng, S.:  
1054 Evaluation of an improved intermediate complexity snow scheme in the ORCHIDEE land surface  
1055 model, *Journal of Geophysical Research: Atmospheres*, 118, 6064-6079, 2013.
- 1056 Wanner, H., Beer, J., Buetikofer, J., Crowley, T. J., Cubasch, U., Flueckiger, J., Goosse, H., Grosjean,  
1057 M., Joos, F., Kaplan, J. O., Kuettel, M., Mueller, S. A., Prentice, I. C., Solomina, O., Stocker, T. F.,  
1058 Tarasov, P., Wagner, M., and Widmann, M.: Mid- to Late Holocene climate change: an overview,  
1059 *Quaternary Science Reviews*, 27, 1791-1828, 2008.



1060 Wohlfahrt, J., Harrison, S. P., and Braconnot, P.: Synergistic feedbacks between ocean and vegetation  
1061 on mid- and high-latitude climates during the mid-Holocene, *Climate Dynamics*, 22, 223-238, 2004.  
1062 Woillez, M., Kageyama, M., Krinner, G., De Noblet-Ducoudré, N., Viovy, N., and Mancip, M.: Impact of  
1063 CO<sub>2</sub> and climate on the Last Glacial Maximum vegetation: results from the ORCHIDEE/IPSL models,  
1064 *Climate of the Past*, 7, 557-577, 2011.  
1065 Zhu, D., Ciais, P., Chang, J., Krinner, G., Peng, S., Viovy, N., Peñuelas, J., and Zimov, S.: The large mean  
1066 body size of mammalian herbivores explains the productivity paradox during the Last Glacial  
1067 Maximum, *Nature Ecology & Evolution*, 2, 640-649, 2018.  
1068 ▲ Zhu, D., Peng, S. S., Ciais, P., Viovy, N., Druel, A., Kageyama, M., Krinner, G., Peylin, P., Ottlé, C., Piao,  
1069 ▲ S. L., Poulter, B., Schepaschenko, D., and Shvidenko, A.: Improving the dynamics of Northern  
1070 ▲ Hemisphere high-latitude vegetation in the ORCHIDEE ecosystem model, *Geoscientific Model*  
1071 ▲ *Development*, 8, 2263-2283, 2015.  
1072  
1073

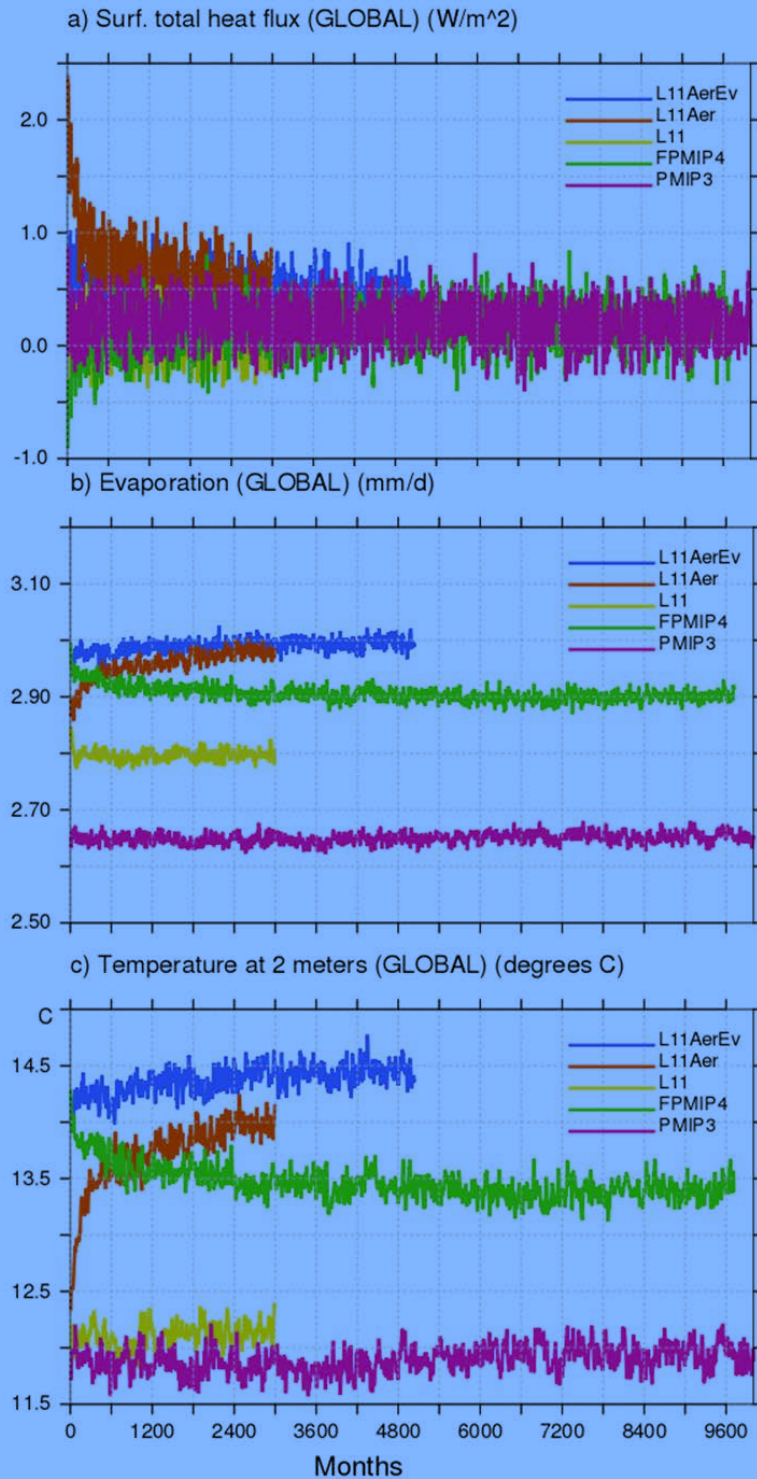


Figure 1: Illustration of the effect of the different adjustments made to produce mid-Holocene simulations with the modified version of the IPSLCM5A-MR version of the IPSL model in which the land surface model ORCHIDEE includes a different soil hydrology and snow models (see text for details). The three panels show the global average of a) net surface heat flux ( $\text{W.m}^{-2}$ ), b) evaporation ( $\text{kg.m}^{-2}$ ), and c) 2m air temperature ( $^{\circ}\text{C}$ ). The different color lines represent the results for the different simulations reported in Table 1.

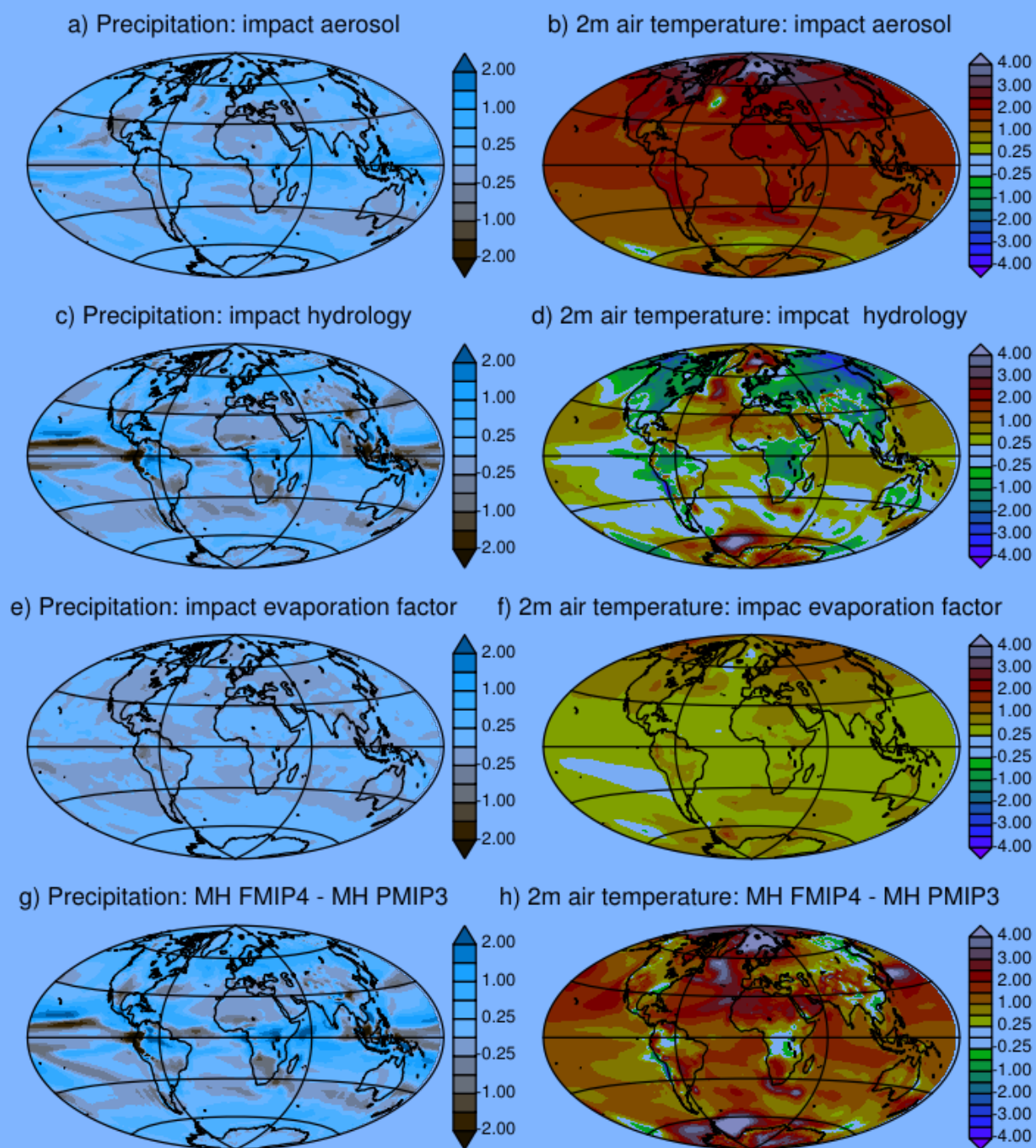


Figure 2: Mid Holocene annual mean precipitation ( $\text{mm.d}^{-1}$ ) and 2m air temperature ( $^{\circ}\text{C}$ ) differences between a) and b) L11Aer and L11, c) and d) L11 and PMIP3, e) and f) PMIP3L11AerEv and L11Aer, and g) and h) FPMIP4 and PMIP3. See Table 1 and text for the details about the different simulations.

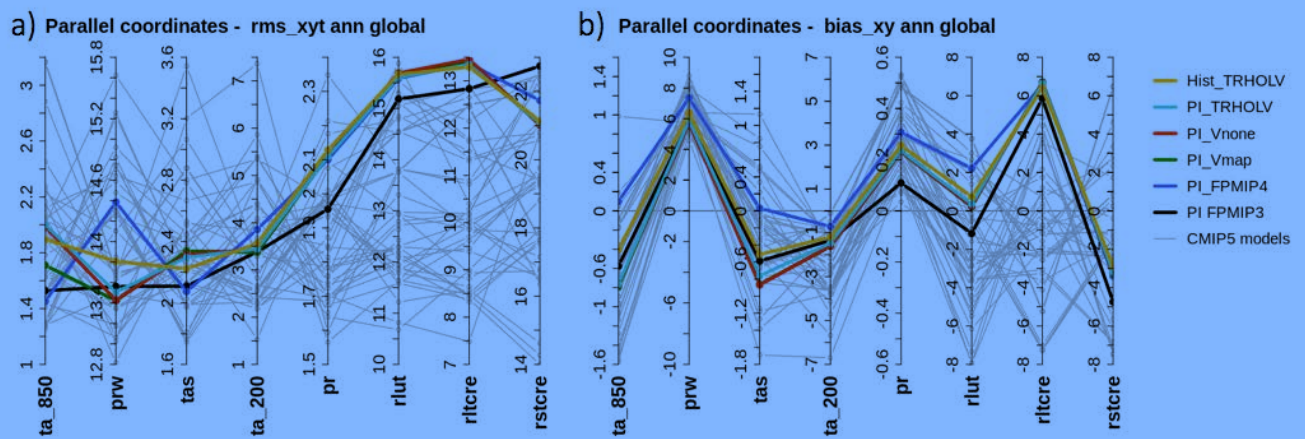


Figure 3. a) Annual mean global model bias ( $\text{bias}_{xy}$ ) and b) spatio-temporal root mean square differences ( $\text{rms}_{xyt}$ ) computed on the annual cycle (twelve climatological months) over the globe for the different pre-industrial simulations considered in this manuscript (colored lines) and individual simulations of the CMIP5 multi-model ensemble (grey lines). The metrics for the different variables are presented as parallel coordinates, each of them having their own vertical axis with corresponding values. In these plots,  $ta$  stands for temperature ( $^{\circ}\text{C}$ ) with  $s$  for surface, 850 and 200 for 850 and 300 hPa respectively,  $prw$  for total water content ( $\text{g}\cdot\text{kg}^{-1}$ ),  $pr$  for precipitation ( $\text{mm}\cdot\text{d}^{-1}$ ),  $rlut$  for outgoing long wave radiation ( $\text{W}\cdot\text{m}^{-2}$ ),  $rltcre$  and  $rltcre$  for the cloud radiative effect at the top of the atmosphere in the short wave and long wave radiation respectively ( $\text{W}\cdot\text{m}^{-2}$ ). See annex A1 for details on the metrics.

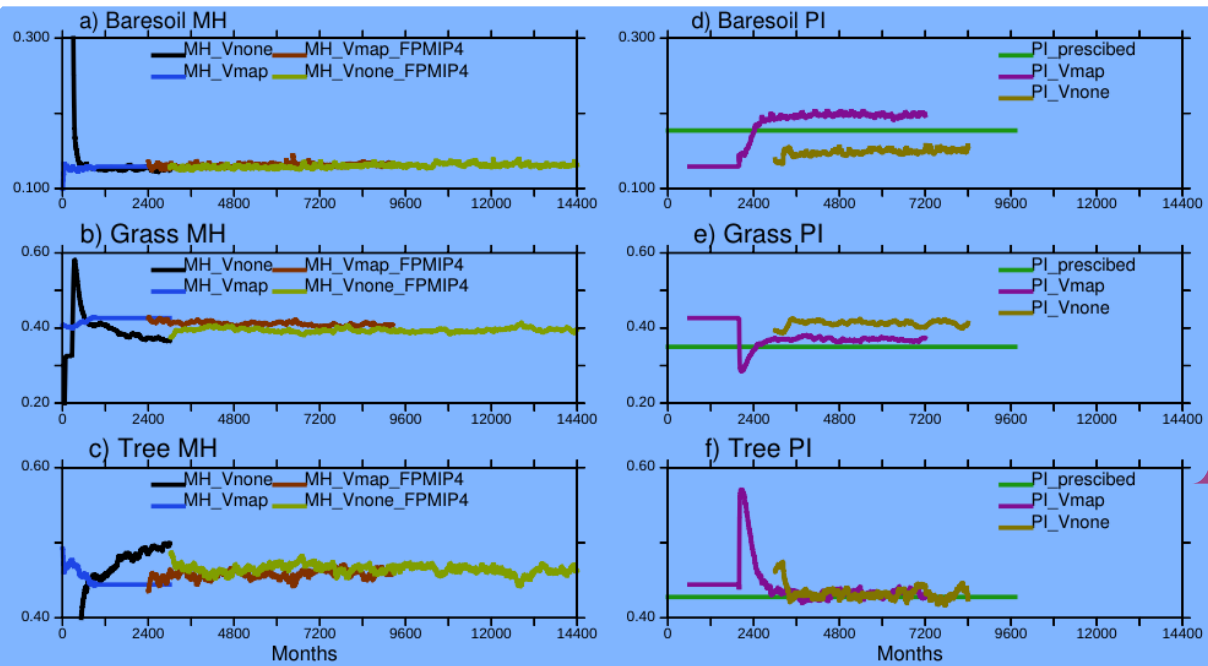


Figure 4. Long term adjustment of vegetation for a) b) and c) mid Holocene (MH) and c), d) and e) preindustrial (PI) climate, when starting from bare soil (Vnone) or from a vegetation map (Vmap). The 13 ORCHIDEE PFTs have been gathered as bare soil, grass, tree and land-use. When the dynamical vegetation is active only natural vegetation is considered. Land-use is thus only present in one simulation, corresponding to a pre-industrial map used as reference in the IPSL model (Dufresne et al. 2013). The corresponding vegetation is referred to as PI\_prescribed. The x axis is in months, starting from 0, which allows to plot all the simulation that have their own internal calendar on the same axis.

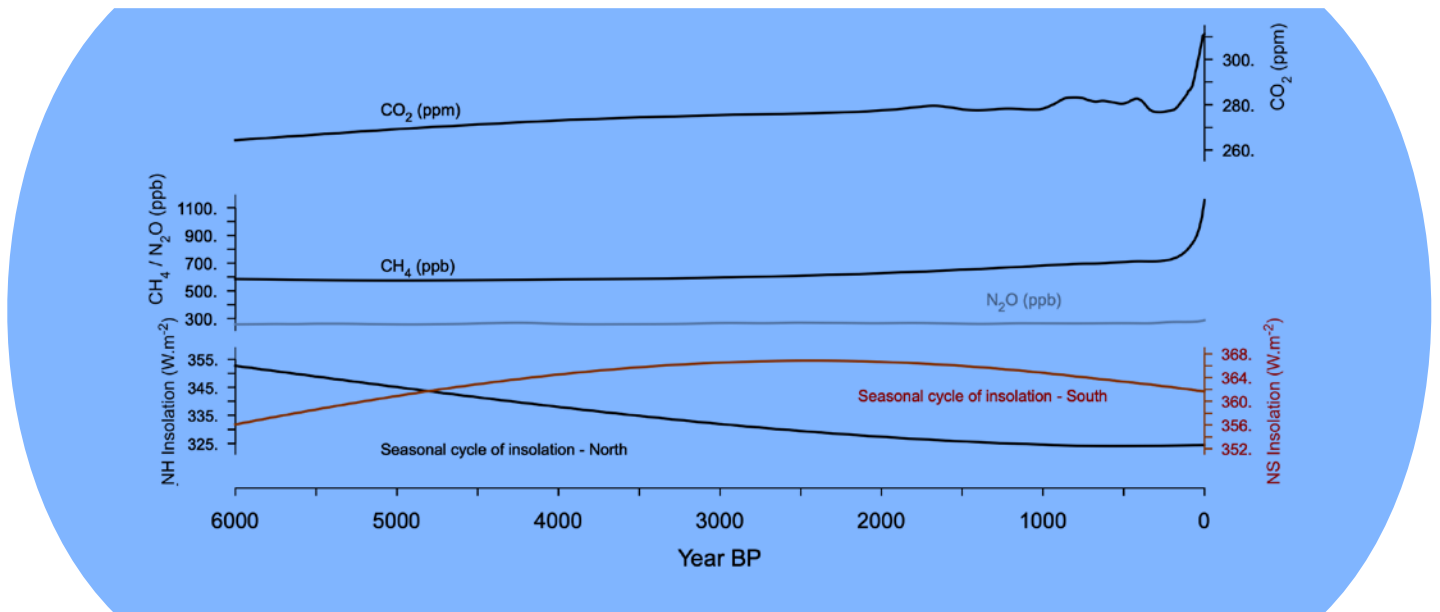


Figure 5: Evolution of trace gases:  $\text{CO}_2$  (ppm),  $\text{CH}_4$  (ppb) and  $\text{N}_2\text{O}$  (ppb), and seasonal amplitude (maximum annual – minimum annual monthly values) of the incoming solar radiation at the top of the atmosphere ( $\text{W}\cdot\text{m}^{-2}$ ) averaged over the northern (black line) and the southern (red line) hemispheres. These forcing factors correspond to the PMIP4 experimental design discussed by Otto-Bliesner et al. (2017).

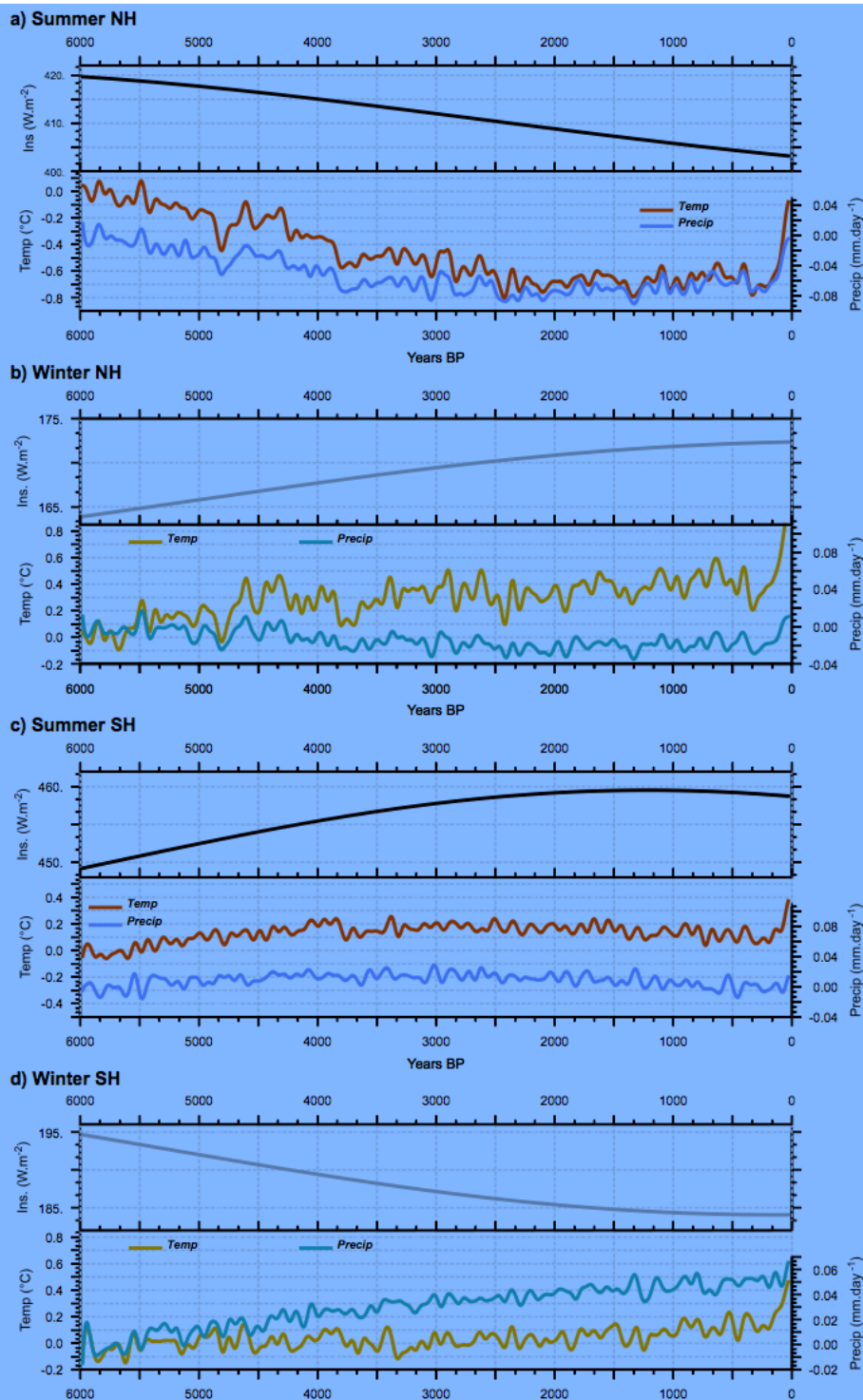


Figure 6. Long term evolution of incoming solar radiation at the top of the atmosphere (TOA)(Wm<sup>-2</sup>, top panel) and associated response of temperature (°C) and precipitation (mm.y<sup>-1</sup>) expressed as a difference with the 6000 year PB initial state and smoothed by a 100 year running mean) for a) NH Summer, b) NH winter, c) SH summer, and d) SH winter. Temperatures are plotted in red and precipitation in blue for summer, and they are respectively plotted in orange and green for winter. NH Summer and SH Winter correspond to June to September averages whereas NH winter and SH summer correspond to December to March averages. All curves, except insolation, have been smoothed by a 100 year running mean.

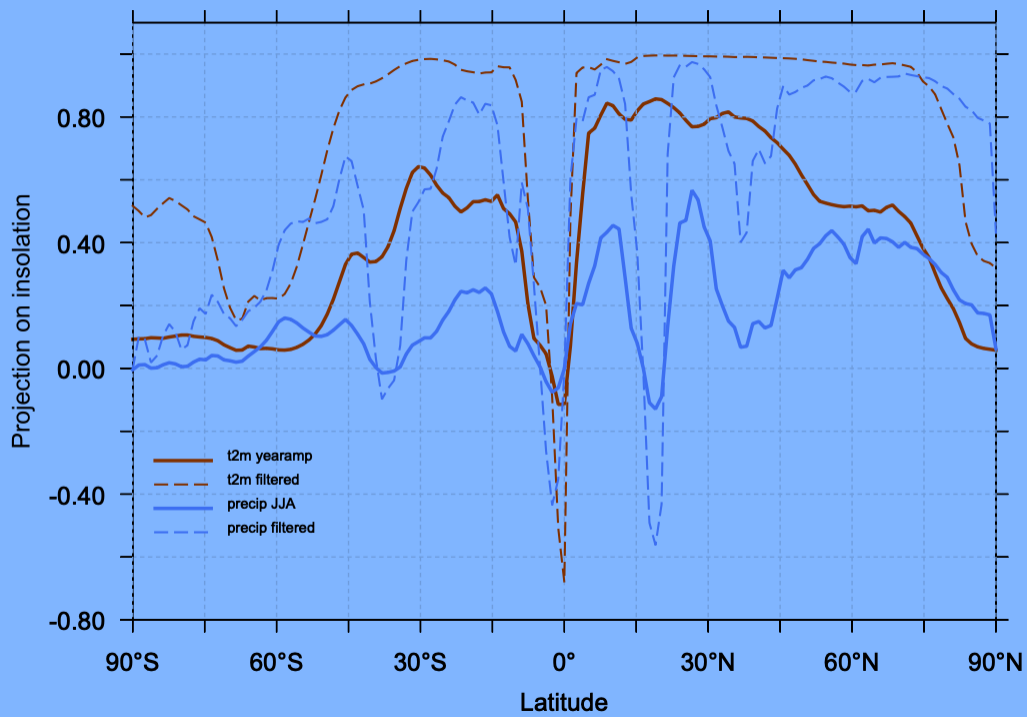


Figure 7: Fraction of the evolution of the seasonal amplitude of temperature (red) and precipitation (blue) represented by the projection of these climate variables on the evolution of the seasonal amplitude of insolation as a function of latitude. The solid line stands for the raw signal and the dotted line for the signal after a 100 year smoothing.



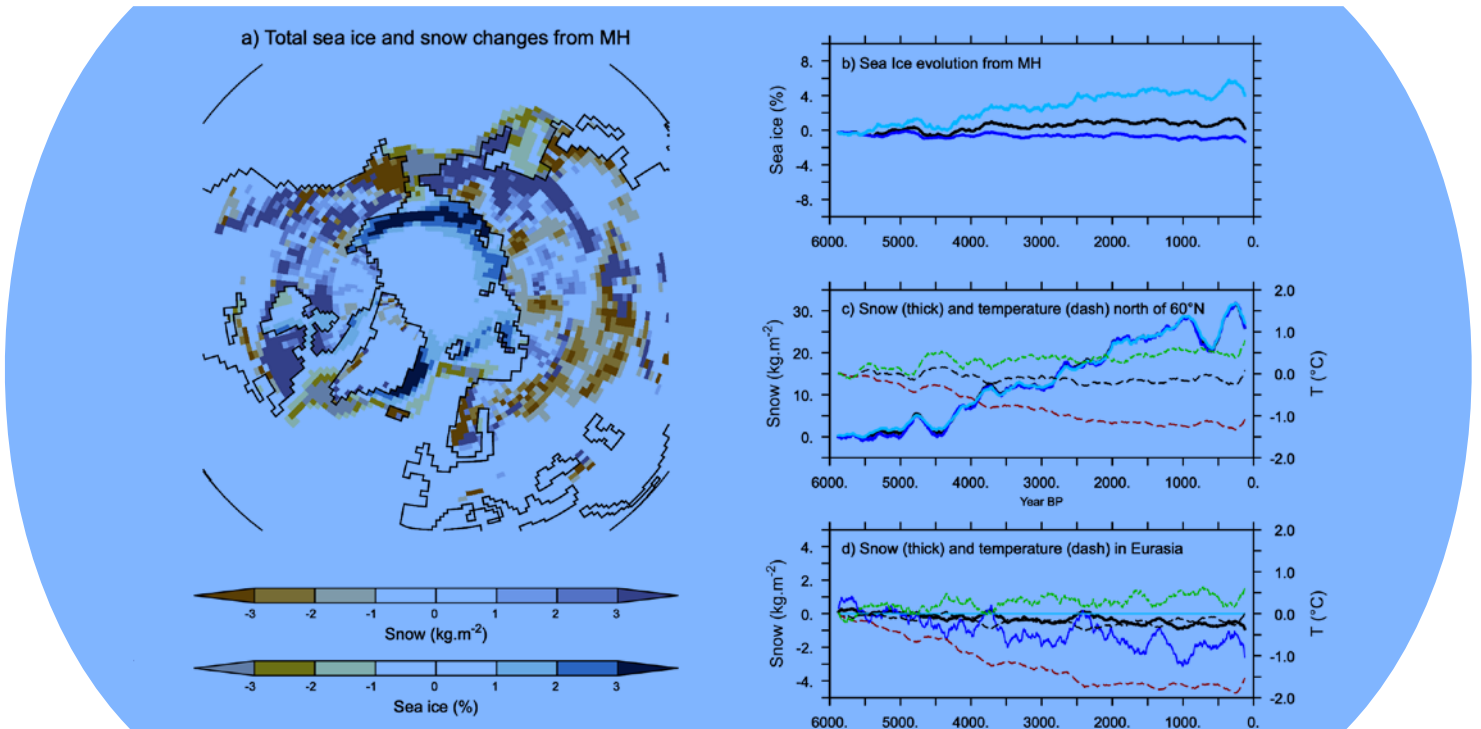


Figure 8: a) total change in snow cover ( $\text{kg m}^{-2}$ ) and sea ice fraction (%) integrated over the last 6000 years, and evolution from the Mid Holocene of annual mean maximum summer and minimum winter values for b) sea ice averages over the northern hemisphere, c) snow (solid lines) and 2-m air temperature (dotted lines) average for all regions north of  $60^{\circ}\text{N}$ , and d) snow and 2m air temperature over Eurasia. In b), c), and d) black, dark blue and light blue stand respectively for the annual mean, maximum and minimum annual monthly values for sea-ice or snow cover, and black, green and red for annual mean, annual minimum and annual maximum air temperature.

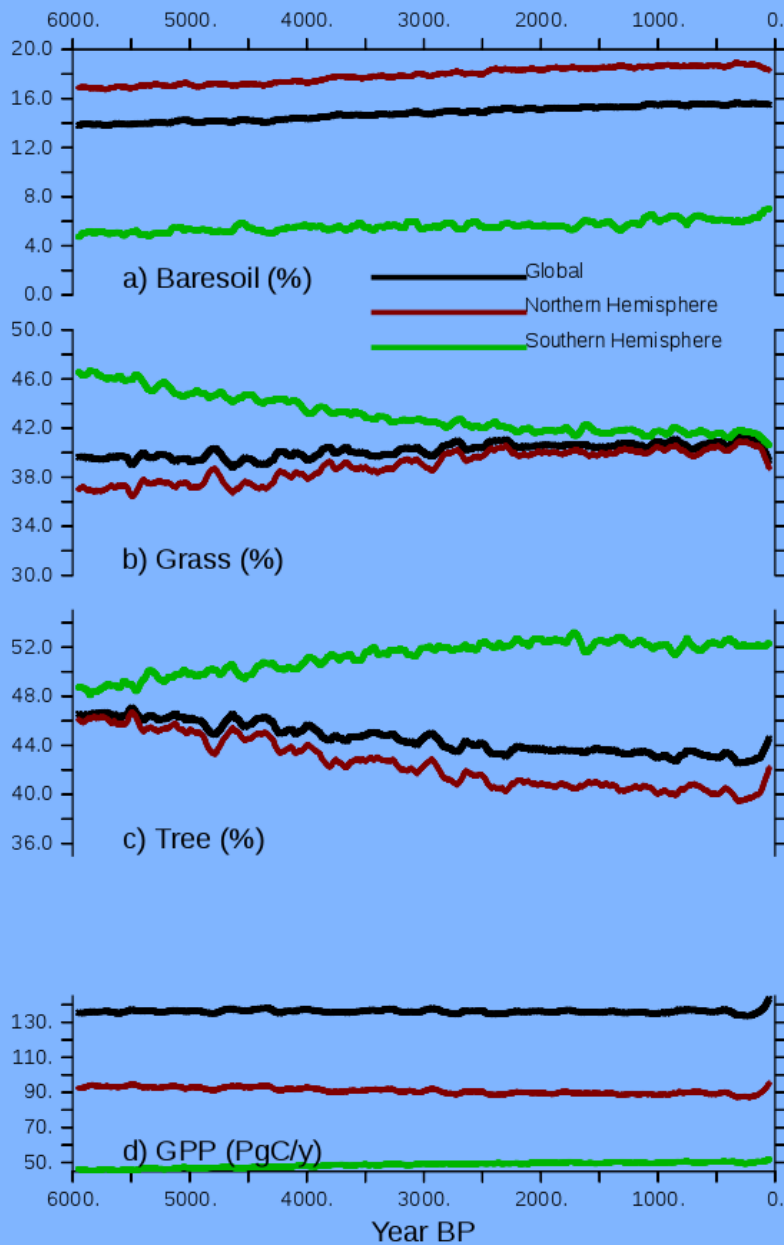


Figure 9: Long term evolution of the simulated a) bare soil, b) grass and c) tree covers, expressed as the percentage (%) of Global, NH or SH continental areas, and d) GPP (PgC/y) over the same regions. Annual mean values are smoothed by a 100 year running mean.

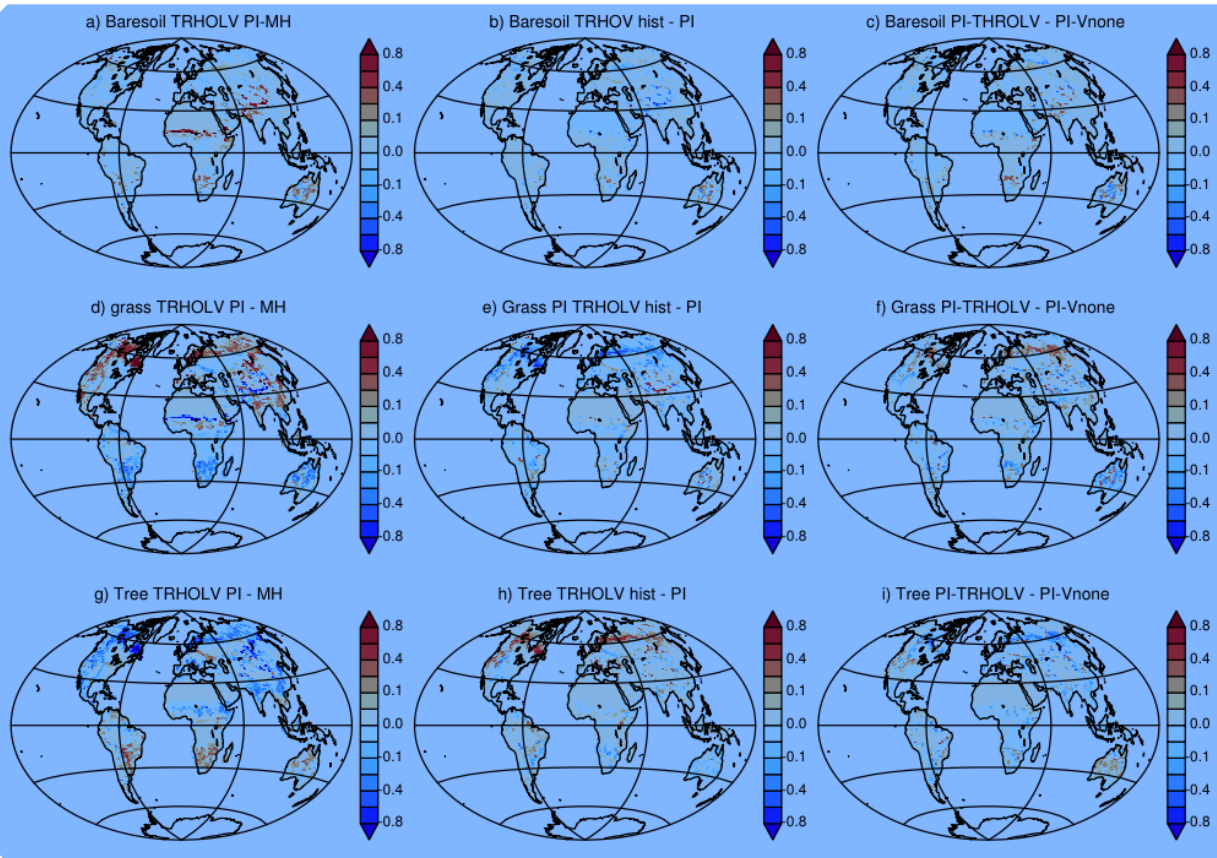


Figure 10: Vegetation map comparing a), d), g) the Mid Holocene (first 50 years) and the pre-industrial (50 year around 1850 AC (last 150 to 100 years) periods of the transient simulation , b), d), h) the differences between the historical period (last 50 years) and the pre-industrial period of the transient simulation and c), f), i) the difference between pre-industrial climate for the transient simulation and the PI-Vnone simulations. For simplicity we only consider bare soil (top), grass

(middle) and tree (bottom).

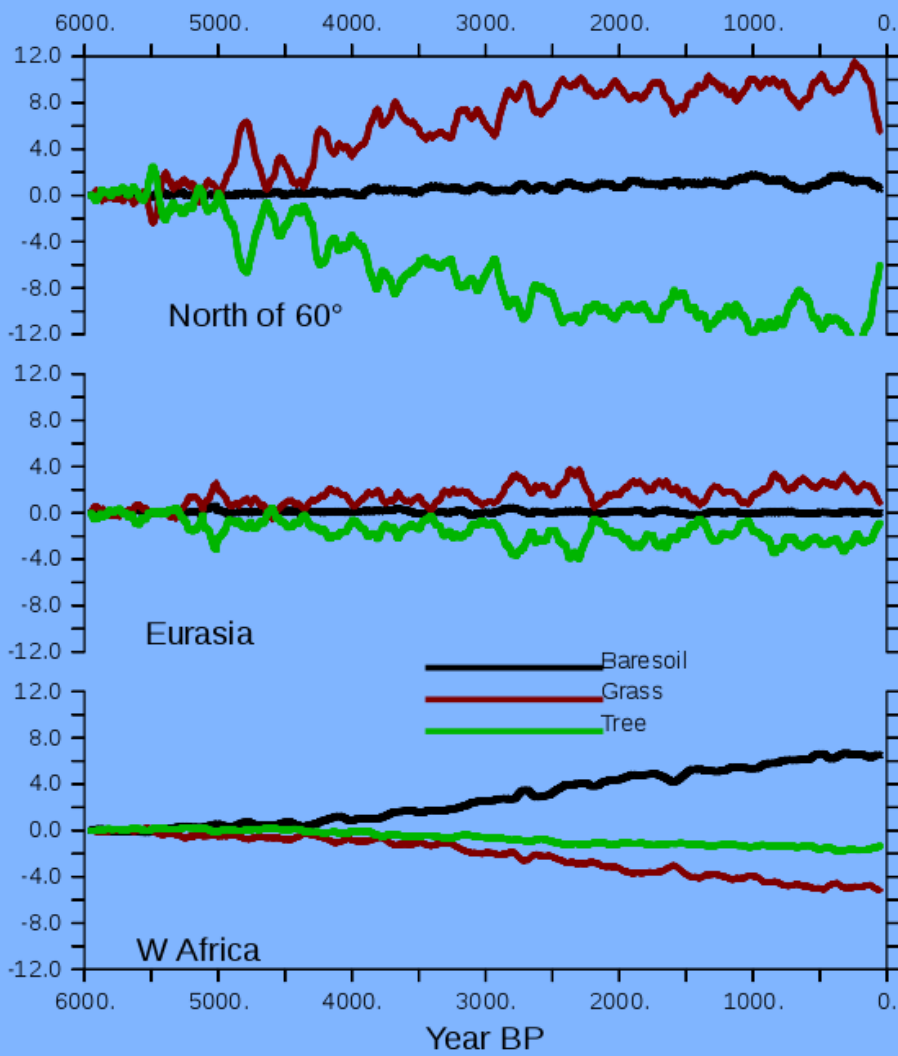


Figure 11: Long term evolution of Bare soil, Grass and Tree, expressed as the % of land cover North of 60°N, over Eurasia and over West Africa. The different values are plotted as differences with the first 100 year averages. A 100 year running mean is applied to the curves before plotting.

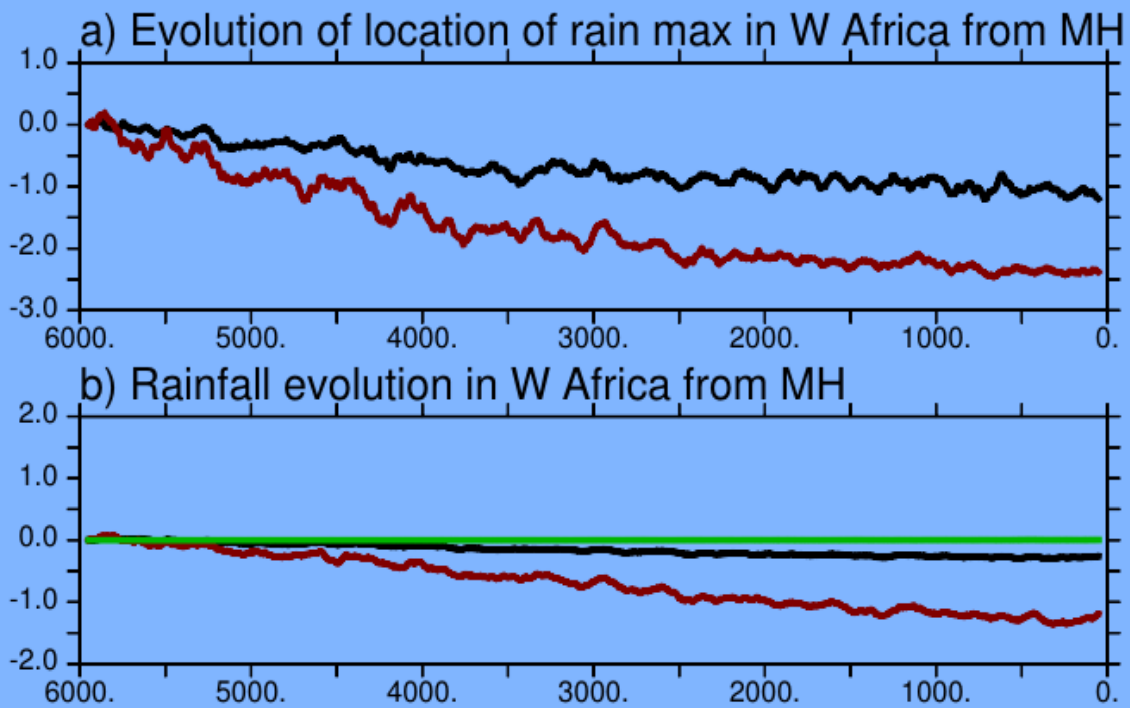


Figure 12. Evolution of a) the location of the West African monsoon annual mean (black) and maximum (red) rain belt in degrees of latitude and b) annual mean (black), minimum (green) and maximum (red) monthly precipitation ( $\text{mm.d}^{-1}$ ) averages over the Sahel region. The first 100 years have been removed and a 100 running mean applied before plotting.

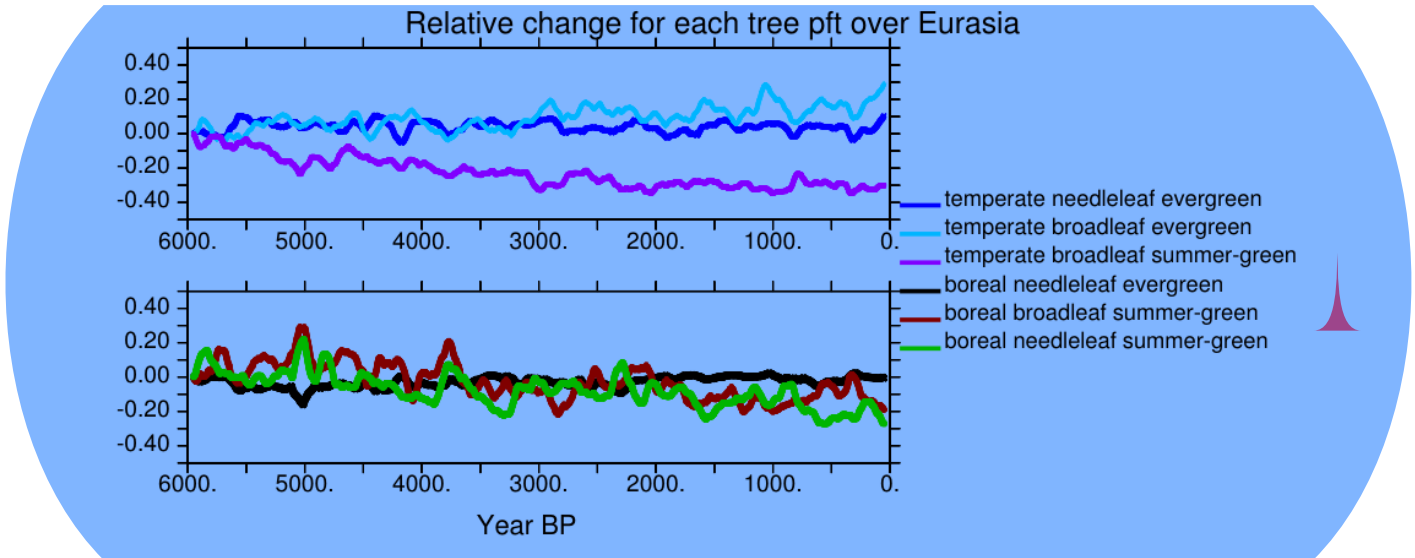


Figure 13: Evolution of the different tree PFTs in Eurasia, expressed as the percentage change compared to their 6000 year BP initial state. Each color line stands for a different PFT. Values have been smoothed by a 100 year running mean.

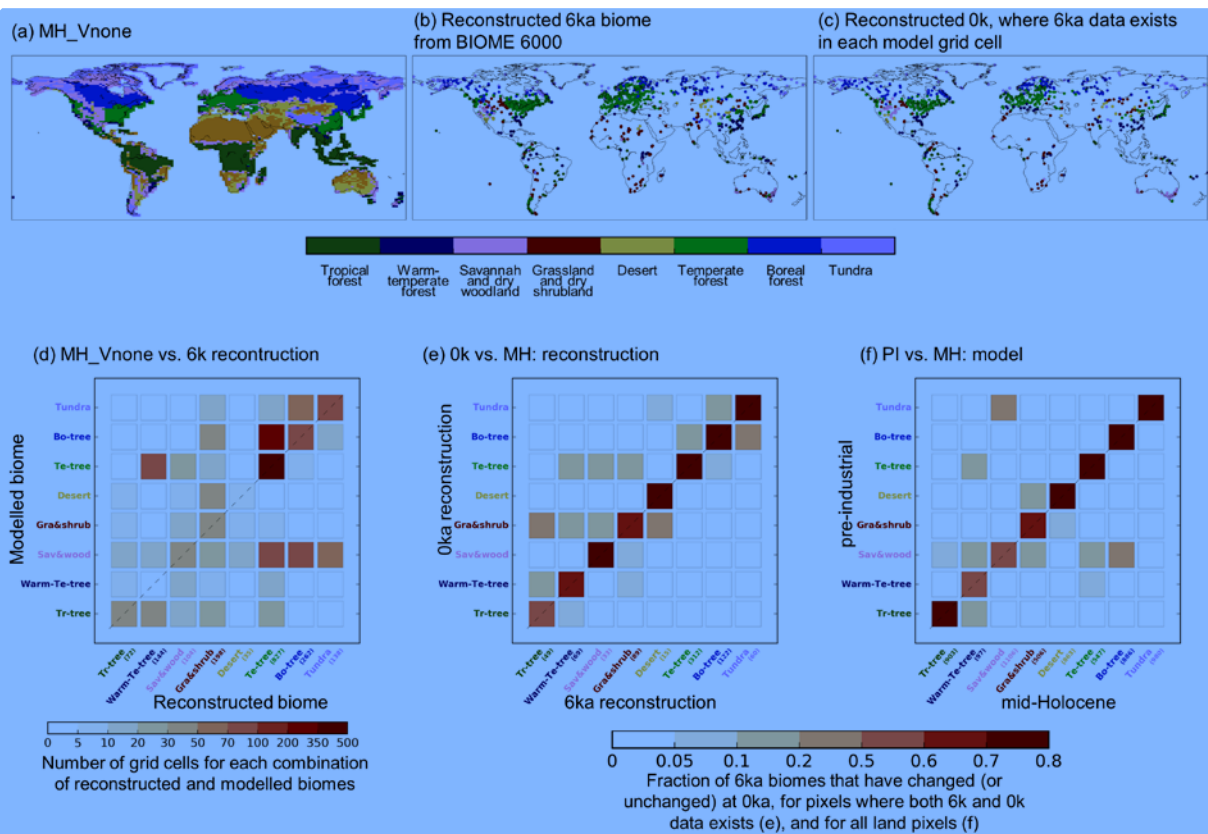


Figure 14: a) Simulated mega-biome distribution by MH-Vnone, converted from the modelled PFT properties using the default algorithm described in Figure A1. b) and c) Reconstructions in BIOME 6000 DB version 1 for the MH and PI periods (Harrison, 2017). d) Number of pixels where reconstruction is available and the model matches (or does not match) the data. Note that multiple reconstruction sites may be located in the same model grid cell, in which case we did not group them so that each site was counted once. Numbers in parenthesis on the x axis in d) represent the number of sites for each biome type. Same as in c) but for the number of matches between e) the BIOME6000 MH (6k) and PI (0k) reconstructions at pollen sites and f) the simulated mega-biomes for MH and PI at each model grid cell.

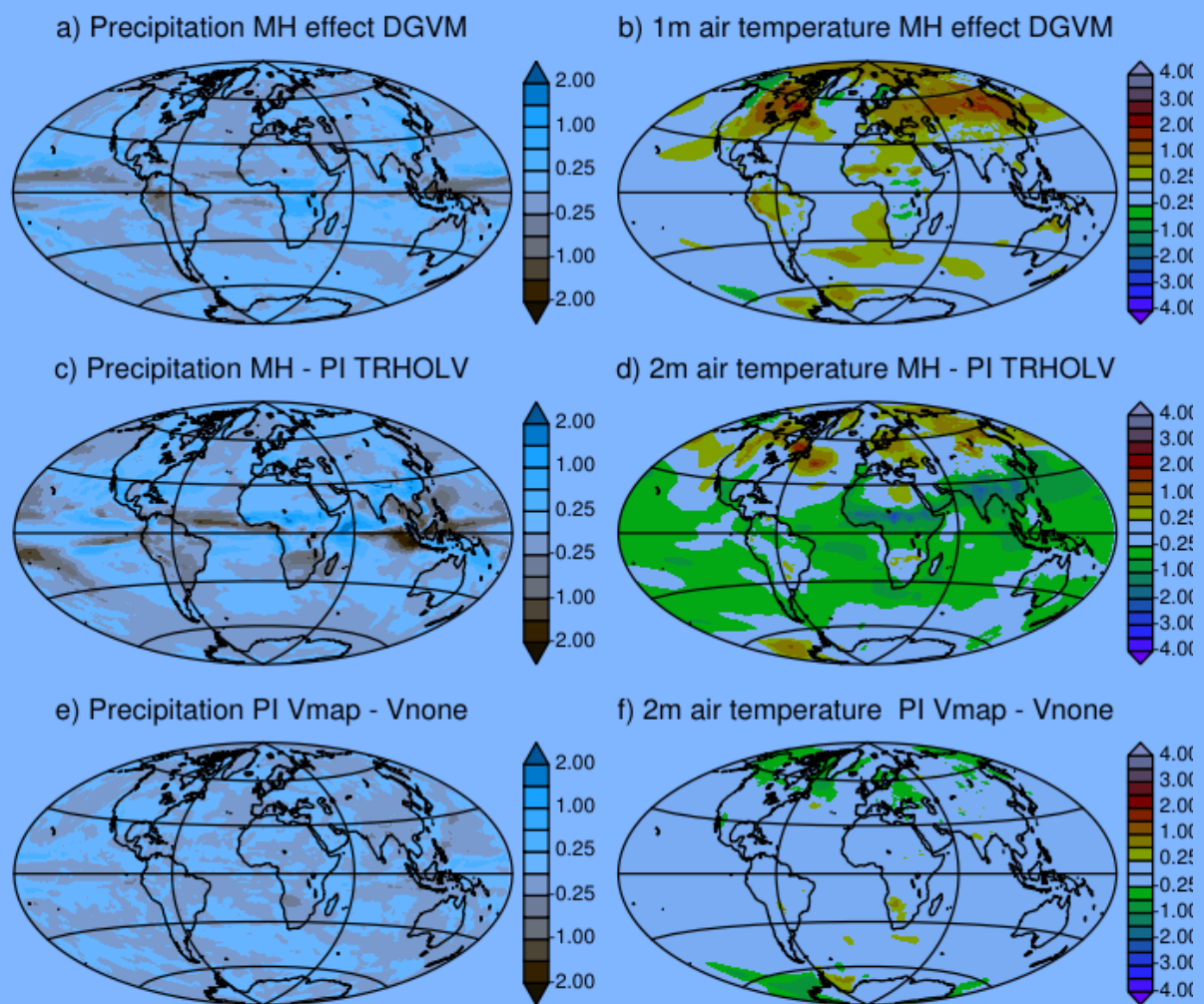


Figure 15: Impact of the dynamical vegetation and initialization of vegetation on the simulated climate. Differences for annual mean a) c) e) precipitation ( $\text{mm.d}^{-1}$ ) and b) d) f) 2m air temperature ( $^{\circ}\text{C}$ ) between a) and b) the MH in the TRHOLV simulation and the MH simulation without dynamical vegetation (MH FPMIP4), d) and d) the mid Holocene and the pre-industrial simulations in the TRHOLV simulation, and e) and f) the two pre-industrial simulations initialized from bare soil (PI-Vnone) or a vegetation map for vegetation (PI-Vmap). See table 2 and text for details on the simulations.



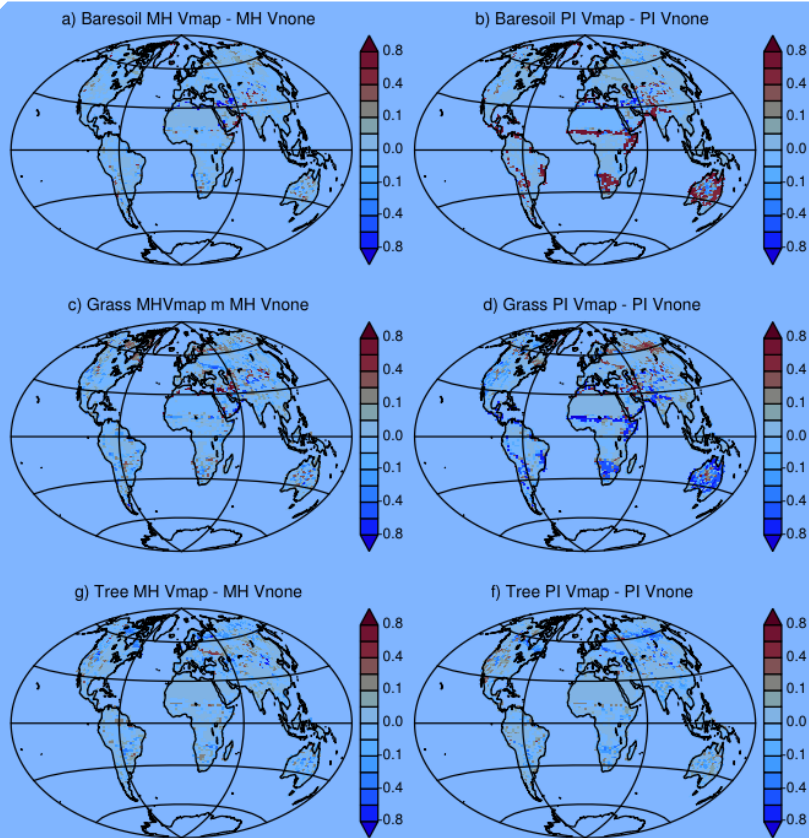


Figure 16: Difference between Vegetation maps obtained with the two different initial states for a) c) e) mid Holocene simulations, b) d) f) pre-industrial simulations. Vmap stands for MH and PI simulations where the mid-Holocene vegetation has been initialized from a vegetation map and Vnone for MH and PI simulations where the mid-Holocene has been initialized from bare soil. For simplicity we only consider fractions of a) b) bare soil, c) d) grass and e) f) trees.

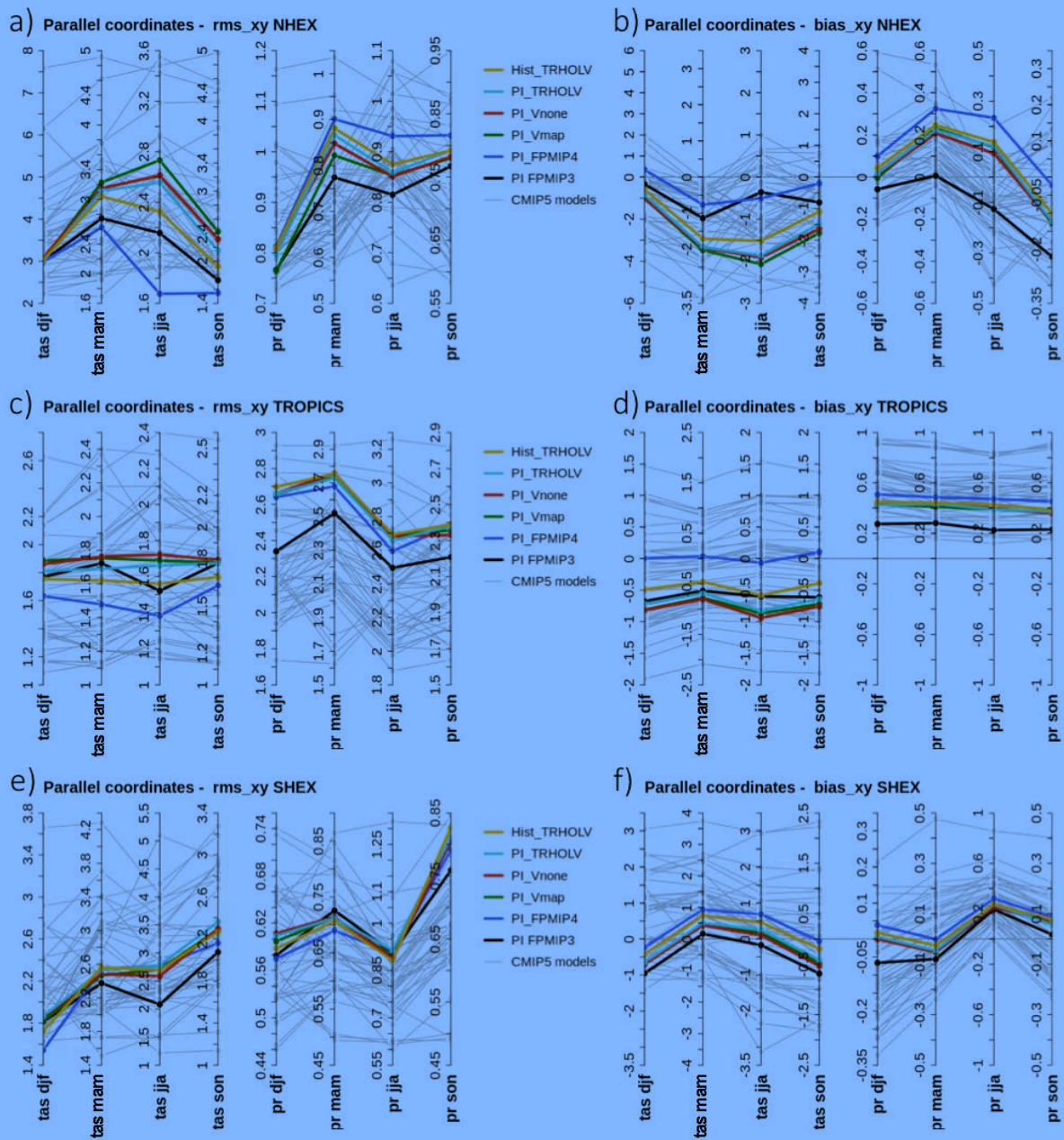
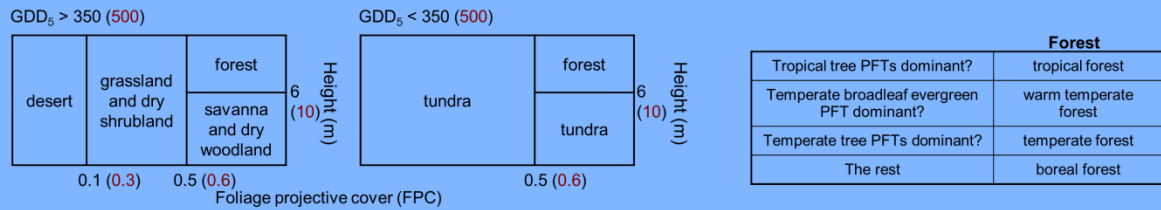
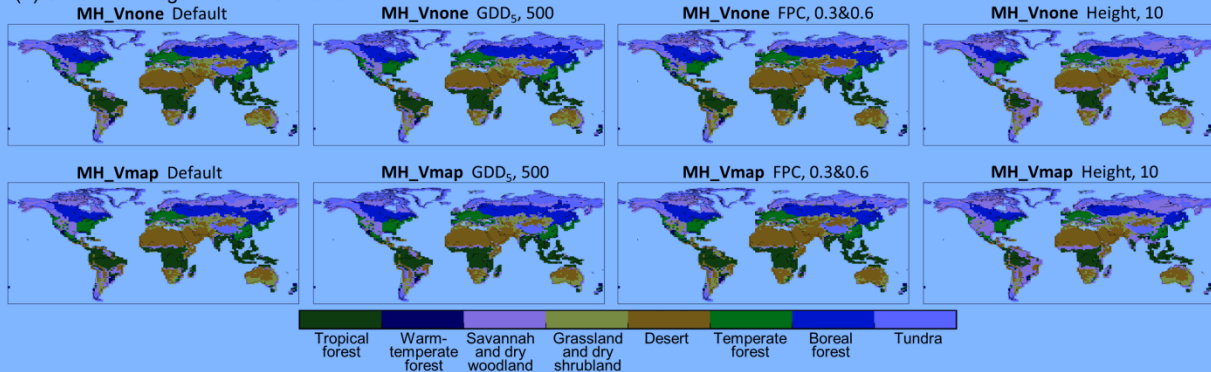


Figure A1: Parallel coordinate representation of metrics highlighting model mean bias (left column) and spatial root mean square differences (right column) against observations for the four climatological seasons (Decembre to February, djf; Mars to May, mam; June to August, jja ; September to November, son) for surface air temperature (tas, °C) and precipitation (mmd<sup>-1</sup>) and Northern Hemisphere extra tropics (NHEx, 20°N-90°N), Tropics (20°S-20°N), and Southern Hemisphere extra tropics (SHEx 90°S-20°S). Each color line stands for a simulations discussed in this manuscript. The results of the different CMIP5 simulations (grey lines) are included for comparison.

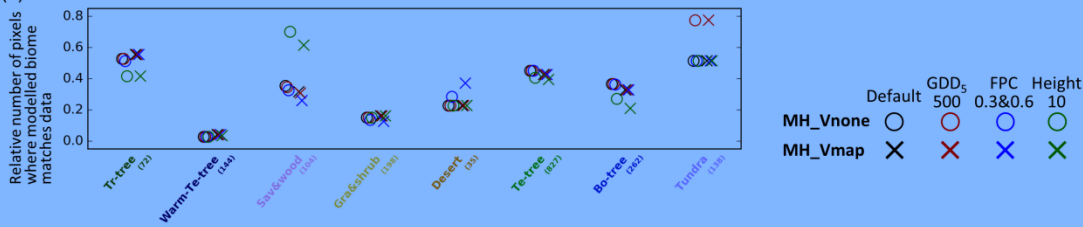
(a) Algorithm to convert the modelled PFT properties into the 8 mega-biomes provided by BIOME 6000



(b) Simulated mega-biome distribution



(c) Percent of correctness



(d) Percent of correctness, TRHOLV (100 years BP)

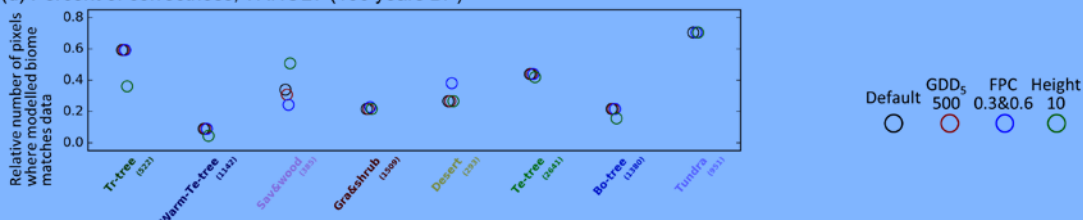


Figure A2 : (a) Algorithm to convert the modelled PFT properties into the eight megabiomes provided by BIOME 6000 DB version 1. The default thresholds (in black) are the same as Zhu et al. (2018), while different values (in red) are tested:  $GDD_5$  (annual growing degree days above 5 °C) of 500 K days (Joos et al., 2004), FPC (foliage projective cover) of 0.3 and 0.6 (Prentice et al., 2011) Height (average height of all existing tree PFTs) of 10 m (Prentice et al., 2011). (b) Simulated megabiome distribution by MH\_Vnone and MH\_Vmap, using different conversion methods in (a). (c) The number of pixels where modelled megabiome matches data for each biome type, divided by the total number of available sites for that biome type.